Aus der Klinik für Allgemeine Pädiatrie, Neonatologie und Kinderkardiologie

der Heinrich-Heine-Universität Düsseldorf

Direktor: Univ.-Prof. Dr. Ertan Mayatepek

Spirometry-Based Reconstruction of Real-time Cardiac MRI: Motion Control and Quantification of Heart-Lung Interactions

Dissertation

zur Erlangung des Grades eines Doktors der Medizin

der Medizinischen Fakultät der Heinrich-Heine-Universität Düsseldorf

vorgelegt von

Lena Maria Röwer

2022

Als Inauguraldissertation gedruckt mit der Genehmigung der Medizinischen Fakultät der Heinrich-Heine-Universität Düsseldorf

gez.:

Dekan: Prof. Dr. med. Nikolaj Klöcker

Erstgutachter/in: Prof. Dr. med. Frank Pillekamp

Zweitgutachter/in: Prof. Dr. med. Gerald Antoch

Drittgutachter/in: PD Dr. med. Inga Voges

Für meine Familie.

Teile dieser Arbeit wurden veröffentlicht:

Röwer LM, Uelwer T, Hußmann J, et al. Spirometry- based reconstruction of real- time cardiac MRI: Motion control and quantification of heart-lung interactions. Magn Reson Med. 2021;86:2692-2702. https://doi.org/10.1002/mrm.28892

Zusammenfassung

Die Atmung beeinflusst die kardiale Magnetresonanztomografie (MRT) sowohl durch die mit der Atmung einhergehende Bewegung des Herzens als auch durch die durch die Atmung induzierten Veränderungen der Herz-Kreislauf-Funktion (Herz-Lungen-Interaktion).

Ziel dieser Machbarkeitsstudie war es, zu untersuchen, wie die Kombination von schneller MRT-Bildgebung (Echtzeit-MRT), einer MRT-kompatiblen Spirometrie und retrospektiver Sortierung toleriert wird, inwieweit hierdurch eine Bildstabilisierung zu erzielen ist und ob so auch eine quantitative Untersuchung der kardialen Funktion und Herz-Lungen-Interaktion während freier Atmung durchgeführt werden kann.

Zu diesem Zweck wurden bei gesunden erwachsenen Probanden (n=4) Echtzeit-MRT-Aufnahmen des Herzens (30 Bilder/s) mit gleichzeitiger MRT-kompatibler Spirometrie durchgeführt. Retrospektiv wurden die MR-Bilder aufgrund der EKG- und Spirometrie-Daten zu neuen Herzzyklen sortiert. Der Patientenkomfort wurde durch einen Fragebogen erfasst. Ausgewertet wurden die Qualität der erzielten Bildstabilisierung, der linksventrikuläre Exzentrizitätsindex als Indikator der Stellung des interventrikulären Septums und die Volumina der beiden Ventrikel der unterschiedlichen Atemphasen zur Beurteilung von Herzfunktion und Herz-Lungen-Interaktion.

Die Beeinträchtigung des Wohlbefindens durch die gleichzeitige Spirometrie war gering. Die Bildstabilisierung wurde durch die Sortierung nach der Atemphase deutlich verbessert.

Die Volumina beider Ventrikel veränderten sich atemabhängig signifikant. Am stärksten beeinflusst wurde das rechtsventrikuläre enddiastolische Volumen (Beginn der Inspiration: 79 +/- 17 ml/m², endexspiratorisch: 98 +/- 18 ml/m²), begleitet von einem Anstieg des rechtsventrikulären Schlagvolumens von 41 +/- 8 ml/m² auf 59 +/- 11 ml/m² und von korrespondierenden Veränderungen des enddiastolischen linksventrikulären Exzentrizitätsindex. Die aus den atemabhängigen Änderungen von Schlagvolumen und enddiastolischen Volumen ermittelte Steigung der Frank-Starling-Kurve entsprach den aus der Literatur bekannten, mit invasiven Methoden erhobenen Werten.

Zusammenfassend verbessert die Kombination aus Echtzeit-MRT, freier Atmung, MRT-kompatibler Spirometrie und retrospektiver, atemabhängiger Sortierung die Bewegungskontrolle und bietet vor allem eine einzigartige, nicht-invasive Möglichkeit der Quantifizierung der Herz-Lungen-Interaktion.

Abstract

Respiration influences cardiac magnetic resonance (MR) imaging both through the heart's movement associated with respiration and through the respiratory-induced changes of cardiovascular function (heart-lung interactions).

The aim of the feasibility study was to investigate how the combination of fast MR imaging (real-time magnetic resonance imaging), MR-compatible spirometry, and retrospective binning is tolerated, to what extent image stabilization can be achieved, and if this also allows quantitative investigation of cardiac function and heart-lung interactions during free- breathing.

For this purpose, real-time MR images of the heart (30 frames/s) with simultaneous MR-compatible spirometry were acquired in healthy adult subjects (n=4). Retrospectively, MR images were binned into new cardiac cycles based on ECG and spirometry data. Patient comfort was assessed by a questionnaire. The quality of image stabilization, the left ventricular eccentricity index as an indicator of the position of the interventricular septum, and the ventricular volumes of different respiratory phases were evaluated to assess cardiac function and heart-lung interactions.

The impairment of comfort by simultaneously measured spirometry was low. Image stabilization was significantly improved by respiratory-based binning.

Volumes of both ventricles changed significantly in the different respiratory classes. The right ventricular end-diastolic volume was influenced most strongly (onset of inspiration: 79 +/- 17 ml/m², end-expiratory: 98 +/- 18 ml/m²), paralleled by an increase of the right ventricular stroke volume from 41 +/- 8 ml/m² to 59 +/- 11 ml/m², and accompanied by corresponding changes of the end-diastolic left ventricular eccentricity index. The slope of the Frank-Starling curve determined from the respiratory-dependent changes in stroke volume and end-diastolic volume was consistent with values known from the literature that were obtained primarily by invasive methods.

In conclusion, the combination of real-time MRI, free-breathing, MR-compatible spirometry, and retrospective respiratory binning improves motion control and, most importantly, provides a unique, noninvasive possibility to quantify heart-lung interactions.

List of abbreviations

bSSFP	balanced steady-state free precession
EI	eccentricity index
EId	end-diastolic eccentricity index
EIs	end-systolic eccentricity index
FLASH	fast low-angle shot
fps	frames per second
HASTE	half acquisition single-shot turbo spin echo
LV	left ventricle
LV-EDVi	left ventricular end-diastolic volume indexed to body surface area
LV-EF	left ventricular ejection fraction
LV-ESVi	left ventricular end-systolic volume indexed to body surface area
LV-SVi	left ventricular stroke volume indexed to body surface area
MR	magnetic resonance
MRI	magnetic resonance imaging
ROI	region of interest
RV	right ventricle
RV-EDVi	right ventricular end-diastolic volume indexed to body surface area
RV-EF	right ventricular ejection fraction
RV-ESVi	right ventricular end-systolic volume indexed to body surface area
RV-SVi	right ventricular stroke volume indexed to body surface area

Index of content

1 Introduction

1.1 Cardiac MRI in pediatric cardiology

Echocardiography is the imaging technique most frequently used in pediatric cardiology. Advantages of echocardiography are its almost ubiquitous availability and its applicability at any age without the need for sedation or anesthesia. It offers a high temporal resolution of 20-80 frames per second and is therefore particularly suitable for imaging fast moving structures like e.g., valves. Temporal resolution of 3D echocardiography is lower, but allows for ventricular function analysis likewise to cardiac magnetic resonance imaging (MRI) (1).

Despite the great advantages of echocardiography, it shows significantly weaker soft tissue contrast (2) and the representation of the heart is sometimes limited by the acoustic window, by bone or air.

Cardiac MRI allows for non-invasive diagnostic free image-plane adjustment (2), which is relevant for an exact anatomical representation and assessment of ventricular volumes, flow measurements in heart-related vessels as well as the left and right ventricular outflow tract (3, 4, 5, 6). These cardiac function parameters are relevant for diagnosing, establishing indications, planning cardiac surgery and subsequent follow-up for children with congenital and acquired heart disease (7, 8). An invasive cardiac catheter examination with radiation exposure can sometimes even be dispensed due to the extensive diagnostic possibilities of cardiac MRI (9).

Although the importance of conventional cardiac MRI in everyday clinical practice in pediatric cardiology is increasing, it still has relevant disadvantages: This includes the need to hold one's breath during cardiac MRI measurements e.g., ventricular volumetry. Breath-holding is only possible from a certain age for pediatric patients and poses a major challenge for even adolescent patients with a history of pulmonary or cardiac disease. Additionally, breath-holding is only possible for a limited time and is associated with a major reduction in patient’s comfort (10, 11). For infants and small children, a cardiac MRI examination is only possible with anesthesia and ventilation, so that this non-invasive method loses its harmless character and makes every day clinical use in infants almost impossible. In addition, holding one’s breath creates an unphysiological state that does not consider the effects on cardiac function in the context of heart-lung interactions (12, 13, 14). Mechanical ventilation based on positive intrathoracic pressure completely reverses the physiological respiratory influence (15). Another disadvantage

of conventional cardiac MRI is the low temporal resolution and the resulting need for ECG-based retrospective gating or prospective triggering to display one heartbeat (16).

1.2 Cine-bSSFP in conventional cardiac MRI

Cardiac cine imaging consists of several static images that are quickly presented as a sequence, enabling the retrospective presentation of a full heart cycle. Due to the natural movement of the heart, it is not possible to obtain all the necessary k-space data for image acquisition during a single cardiac cycle. Therefore, signals to complete k-space filling must be recorded during several heart cycles and must be interpolated afterwards (16, 17). The MR data acquisition is linked to the temporal information of the heart cycle, provided from the ECG via prospective triggering or retrospective gating. In prospective triggering, certain k-space data lines are acquired specifically for a cardiac phase during a cardiac cycle. For this, one k-space is assigned to each cardiac phase (16) **(Figure 1)**.

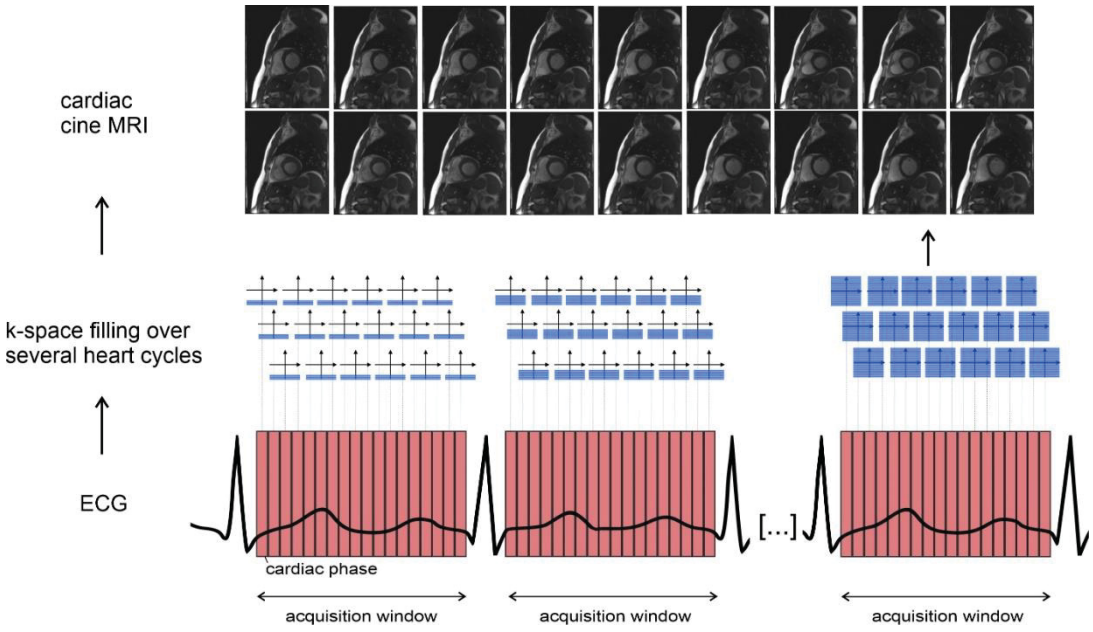

Figure 1. Prospective triggering.

The cardiac cycle is divided in several phases (red) based on the mean RR-interval. Each phase is assigned a defined segmented k-space, which is filled line by line over several heartbeats (blue). The data acquisition begins shortly after the R-wave and ends before the next R-wave based on a defined average RR-interval. A disadvantage of prospective triggering is the lack of data attainment during the time of the QRS complex. Filled k-spaces serve as basis for MR image reconstruction (modified from Rigdway JP (16)).

In retrospective gating, k-space lines are acquired continuously during a cardiac cycle. Based on the associated time after the R-wave, these are subsequently assigned to specific cardiac phases. The data acquisition is performed over several heartbeats until enough k-space data are available for all heart phases (16) **(Figure 2)**.

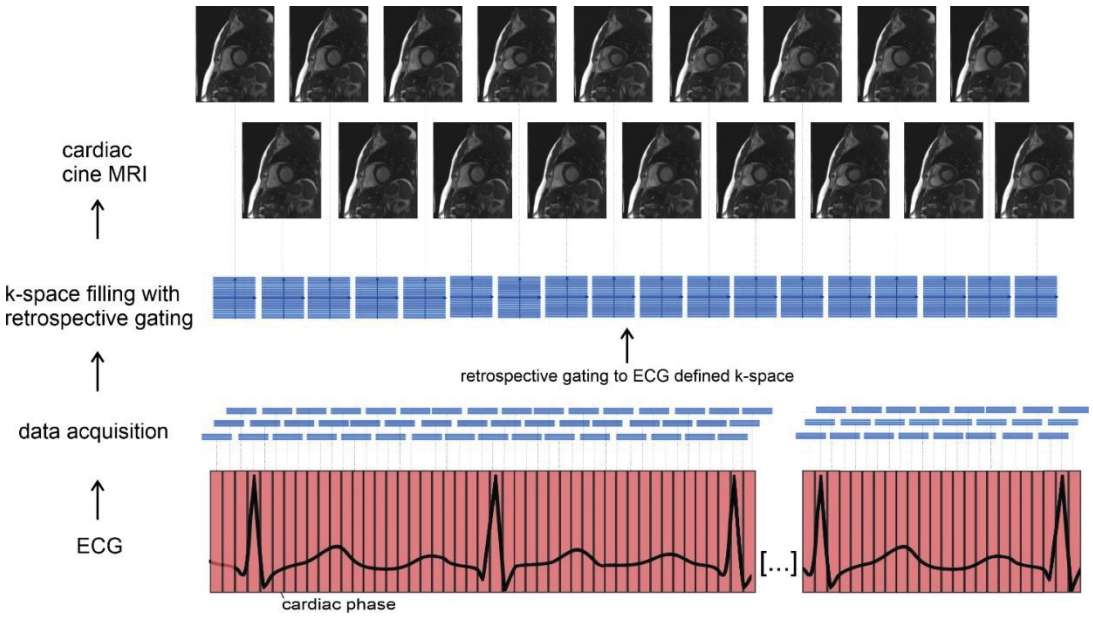

Figure 2. Retrospective gating.
MRI data are acquired continuously during cardiac cycles. These are retrospectively assigned to k-spaces (blue) from specific cardiac phases (red) based on the associated time after the R-wave. Filled k-spaces serve as basis for the subsequent MR image reconstruction (modified from Rigdway JP (16)).

In addition to the heart's own movement, the respiratory-induced displacement of the heart must be considered to provide high image quality and to prevent moving artefacts. This is typically achieved by breath-holding (16, 17).

Although cardiac cine SSFP MRI suffers from disadvantages like the need for interpolating of cardiac cycles and data acquisition under unphysiological conditions, it represents the current MRI standard for analyzing cardiac function in adults (18) and for the examination of children with congenital heart defects (19).

1.3 Real-time MRI of the heart

1.3.1 Relevance of real-time MRI

The importance of real-time MRI and other fast imaging techniques increased over the last years. The relevance of this method is reflected by the number of publications related to real-time MRI and other fast imaging techniques **(Figure 3).**

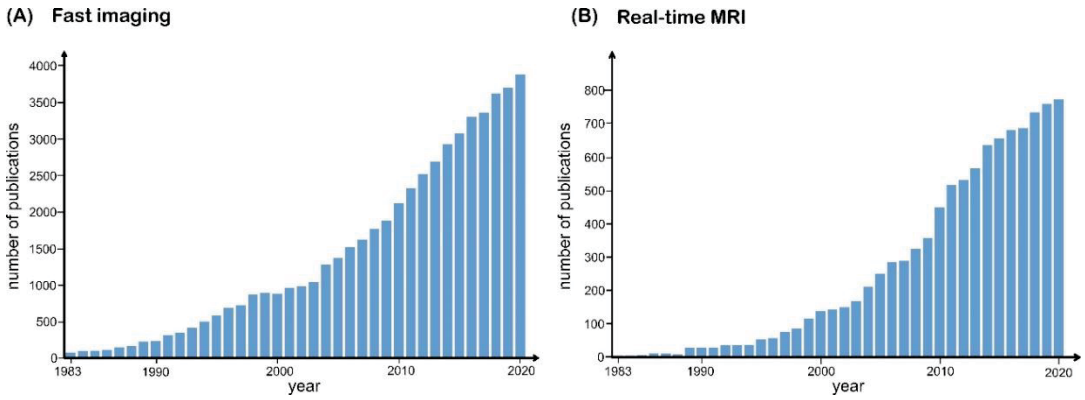

Figure 3. Relevance of fast imaging techniques and real-time MRI.
The number of publications that can be found when searching for fast imaging (A) or real-time MRI (B) on pubmed increased continuously over the last years demonstrating the relevance and importance of these topics.

1.3.2 Methodological aspects and advantages of real-time MRI

Real-time MRI is a technique that was developed by Jens Frahm and his research group in Göttingen in 2010 (20). Real-time MRI is based on rapid MRI studies that were done already in 1985 when the Frahm group developed low-flip angle gradient-echo MRI, the FLASH method, which reduced the acquisition time for a single high-quality image significantly to a few hundred milliseconds (21).

In addition to this development, the data acquisition was further accelerated by undersampling of the image raw data. For this, k-space is filled by radial scanning (20) **(Figure 4)**. Radial trajectories rely on frequency-encoding gradients covering low- and high-spatial frequencies. Especially, the center of k-space is densely sampled and therefore, most of the relevant image information is covered (22). The number of spokes can be reduced for shorter acquisition times without image blurring or aliasing (20). Thereby, radial encoding schemes are attractive for fast imaging and undersampling (22).

A novel image reconstruction technique referred to as “regularized nonlinear inversion” is then used for the generation of real-time MR images (20) **(Figure 4)**. The conventional image computation by Fourier transformation is replaced by the solution of a nonlinear inverse problem. For the acquisition of real-time MRI, the iterative numerical method can be decisively improved by the fact that two immediately successive images of a film have very high similarity (temporal regularization). Thereby, fast imaging with 30-50 fps is enabled (22).

Real-time MRI achieves unique advantages for the representation of the heart: Cardiac cycles are presented without the need for repeated measurements and data interpolation for image reconstruction to display one heartbeat. Therefore, significantly shorter acquisition times are possible. Thus, data acquisition can be done during free-breathing. This allows for the examination of small children without the need of anesthesia or mechanical ventilation and most importantly enables evaluation of the heart function under physiological conditions and even allowing for the quantification of heart-lung interactions (22, 23).

Despite the highly relevant advantages, the analysis of cardiac real-time MRI suffers from respiratory-induced motion, aggravating the subsequent clinical evaluation. To establish cardiac real-time MRI in everyday clinical practice further development of evaluation methods is required.

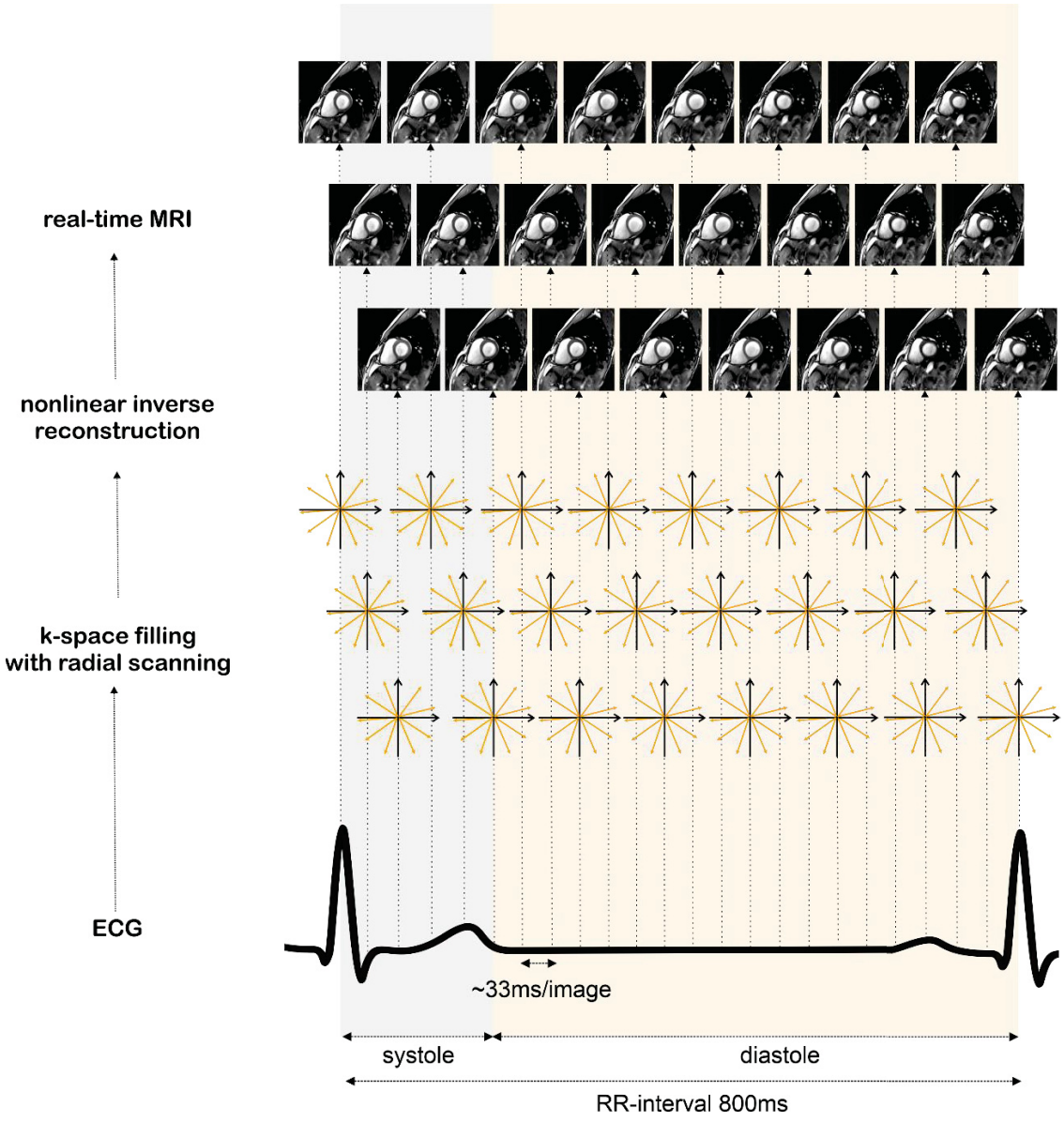

Figure 4. Real-time MRI.

Real-time MRI offers the unique opportunity to acquire heart cycles without data interpolation by using radial scanning with 9 spokes (yellow) for k-space filling and nonlinear inverse reconstruction. Thereby, sampling rates of 33ms/image are possible for covering cardiac cycles.

1.3.3 Real-time volumetry

The volumetric analysis of the ventricles represents a relevant parameter for the assessment of cardiac function. Accordingly, a volumetry MRI sequence is one of the basic measurements of every cardiac MRI examination.

Every cardiac MRI exam starts with the exact determination of the heart's position and orientation derived from localizer MRI sequences **(Figure 5 Part A)**. Subsequently, retrospective two-chamber and four-chamber view cine stack are acquired for planning the short axis stack. The slices covering the ventricles are oriented perpendicular to the septum (yellow lines) **(Figure 5 Part B)**.

With the help of the short-axis data set, the entire volume of the right and left ventricle is covered **(Figure 5 Part C).** Left ventricular endocardial and epicardial contours and right ventricular endocardial contours are provided by the analysis software.

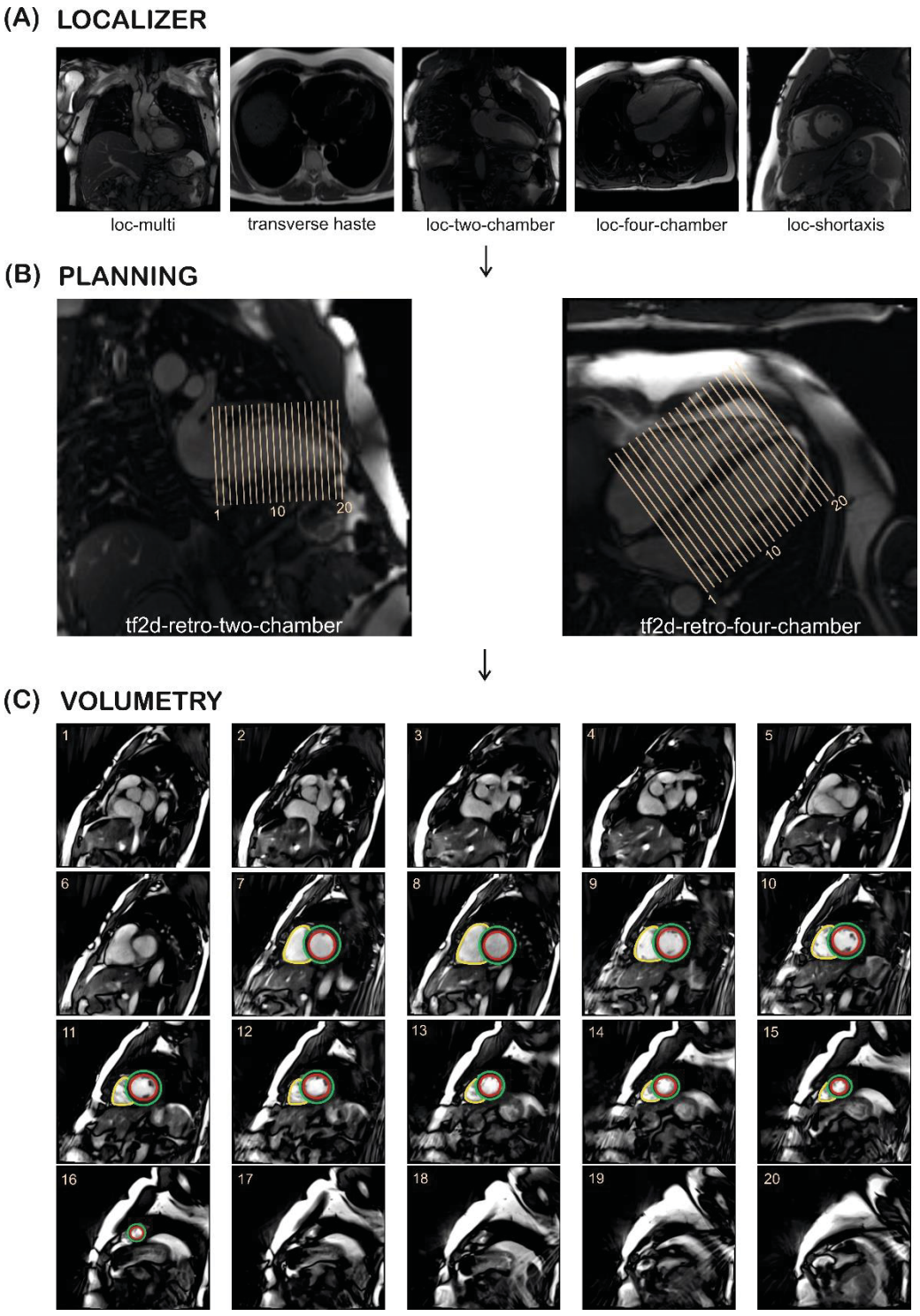

Figure 5. Cardiac volumetry.

A) Localizer images as basis for planning the retrospective two- and four-chamber-view cine stacks (loc-multi, transverse HASTE (half acquisition single-shot turbo spin echo), loc-two-chamber, loc-four-chamber, loc-shortaxis).

B) Retrospective two-and four-chamber-view cine stacks serve as basis for planning the 20 slices of the short axis stack perpendicular to the septum (yellow lines).

C) Images of 20 slices covering the whole ventricles are acquired for the analysis of the left and right ventricular real-time volumetry.

Right and left ventricular volumes and left ventricular mass are calculated from the epicardial and endocardial contouring area and the slice thickness based on three-dimensional reconstruction (24) **(Figure 6)**.

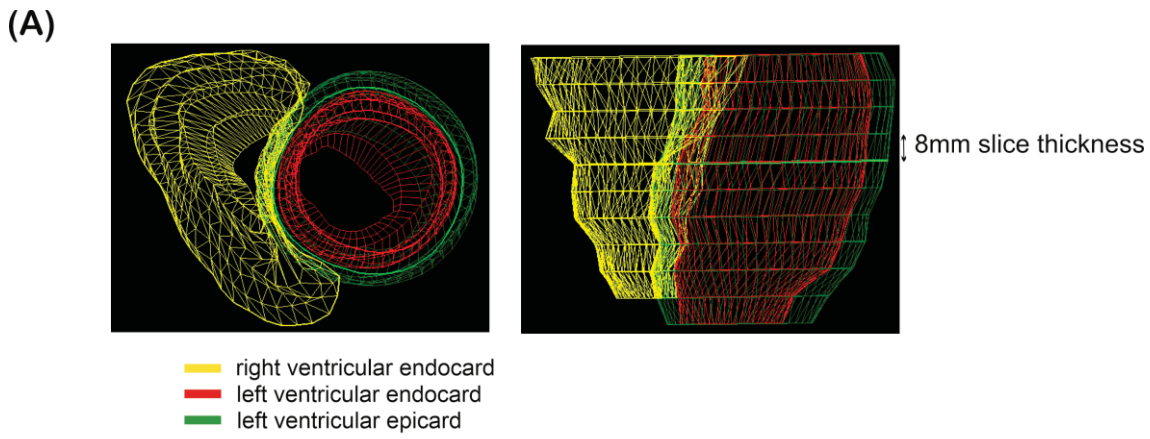

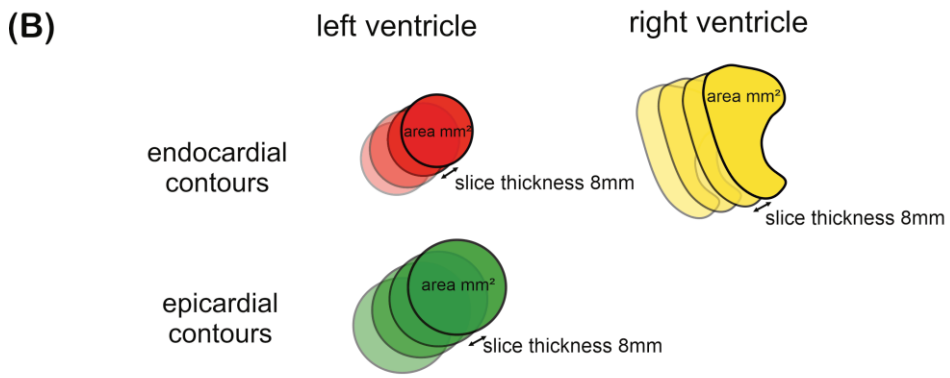

volume calculation based on 3D reconstruction:

V= (A1+A2+A3+.....+A20) x 8mm slice thickness

A= endocardial area in mm² of slice 1-20

Figure 6. Ventricular volume calculation.

A) 3D-model visualizing the contours of the ventricles.

B) Right and left ventricular volumes are calculated by multiplying slice thickness and the sum of the area of the endocardial contours.

Respiratory-induced through-plane motion of the heart results in a change of the slice's location in the short axis stack during free-breathing **(Figure 7)** disturbing the selection of the correct plane.

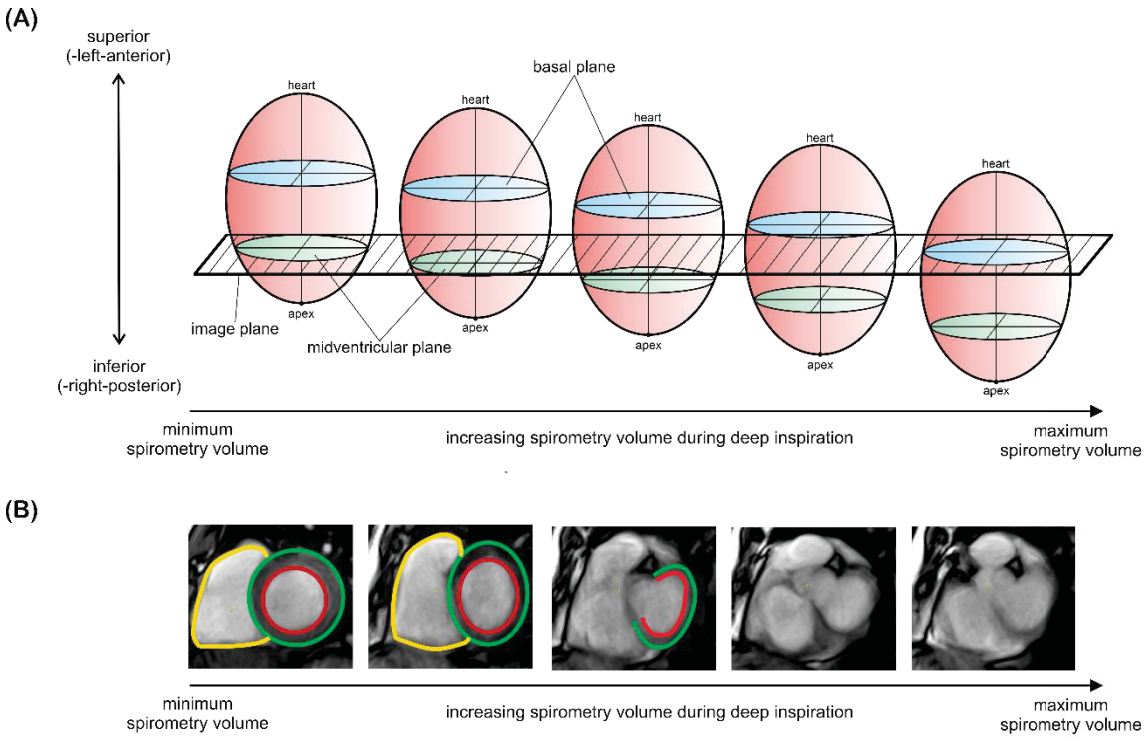

Figure 7. Through-plane motion.

Schematized anatomy of the heart with a midventricular plane (green), a basal plane (blue) and a corresponding image plane. Through-plane motion during deep inspiration causes a defined image plane that is located midventricular to move basally (A). Thereby, the volumetric assessment is disturbed (B).

1.4 Physiological heart-lung interactions during free-breathing

Respiration has a major impact on the heart function resulting from physiological heart-lung interactions.

The heart and lungs are inseparably connected due to their combined location in the thorax cavity. Physiological intrathoracic pressure changes during the respiratory cycle influence venous blood volume distribution, direct ventricular interactions as well as the ventricular afterload (14, 25).

1.4.1 Respiratory influence on cardiac volumes

The impact of preload on cardiac function is well explained by the Frank-Starling law: During inspiration, the decreasing pleural pressure leads to an increased venous return due to the negative pressure difference between the right heart surrounded by the pleural pressure and the mean afferent inferior caval vein surrounded by the intraabdominal pressure (14). The right ventricular end-diastolic preload induces a higher initial sarcomere lengthening. Increased sarcomere lengthening causes a titin modulated reduction of interfilament lattice spacing and triggers the “on-off” equilibrium of the thin filament state. This results in an increased number of myosin attaching to actin. Thereby an increase in active force with an increasing sarcomere length within the physiological range (i.e., ~1.7-2.2 µm) is attained (26) **(Figure 8A)**. Due to the higher tension, an increasing intraventricular pressure and rising right ventricular stroke volume can be achieved demonstrated by an increase in pressure-volume work **(Figure 8B)**. In contrast to the increasing of the right ventricular stroke volume, the left ventricular stroke volume decreases during inspiration. The main reason for this decrease is an increasing afterload due to the lower intrathoracic pressure relative to the higher pressure in extrathoracic compartments (27). In addition, inspiration causes a decrease in left ventricular compliance, resulting from interventricular interactions, effecting a decreased LV preload (27, 28).

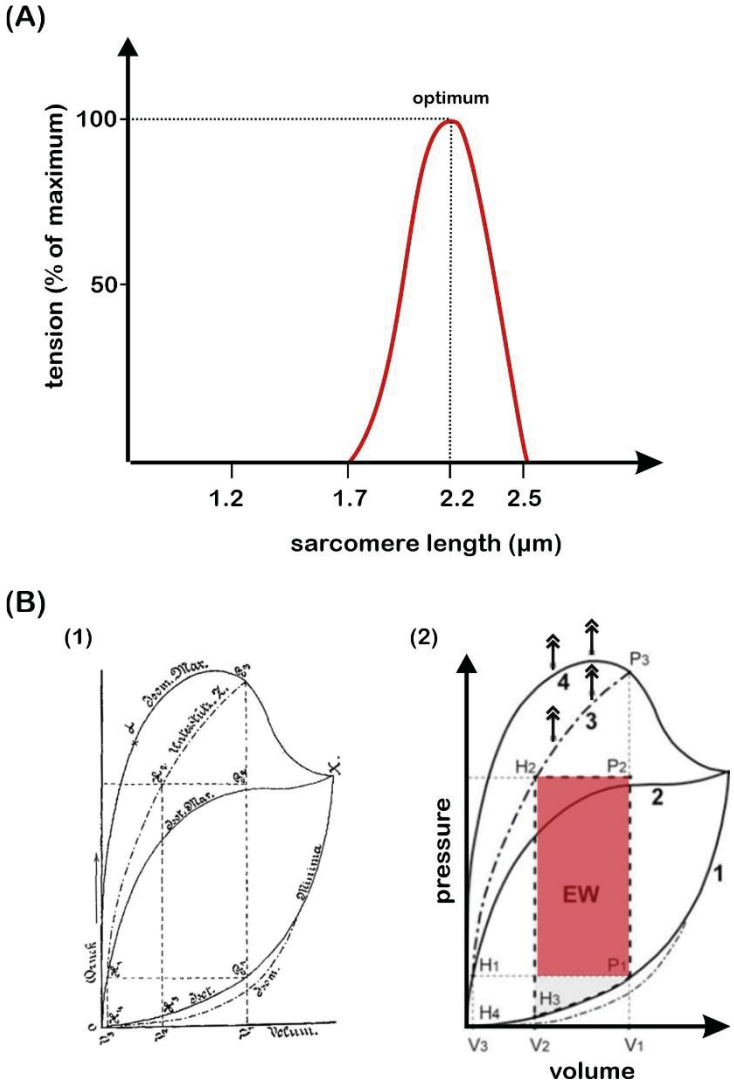

Figure 8. Frank-Starling mechanism.

A) Influence of the sarcomere length on muscle tension (modified from Sequiera V et al. (29)). An increasing sarcomere length up to a maximum pre-expansion of 2.2 µm in cardiomyocytes leads to an increase of tension and contractility.

B) Regulation of heart function with increased preload by the Frank-Starling law (modified from Kuhtz-Buschbeck JP et al. (30)).

1. Otto Frank's pressure volume diagram, as published in 1899.
2. Otto Frank's diagram as schematized version: A higher ventricular volume load results in an increase of ventricular pressure following the distension curve of the minima (1). Consequently, higher isotonic maxima (curve of the isotonic maxima (2)) and higher isometric maxima (curve of the isometric maxima (4)) can be reached, leading to an increased pressure-volume work (shaded area EW= external pressure-volume work). The physiological combination of the isometric and isotonic contraction results in the curve of the after loaded twitches (3). The small arrows present the positive influence of digitalis on the curve of after loaded twitches (3) and the curve of isometric maxima (4).

1.4.2 Direct ventricular interactions during free-breathing

The right and left part of the heart are surrounded by non-distensible fibrous pericardium, limiting acutely occurring extreme dilatation. The right and left ventricle are solely separated by the flexible muscular interventricular septum. An increasing end-diastolic right ventricular volume results in a septal shift to the left ventricle and provides a physiological change of the left ventricular eccentricity index in end-diastole (27) **(Figure 9)**. Therefore, the changes of the left ventricular shape result in a negative effect on the left-ventricular pressure-volume relationship, reducing left ventricular stroke volume (25).

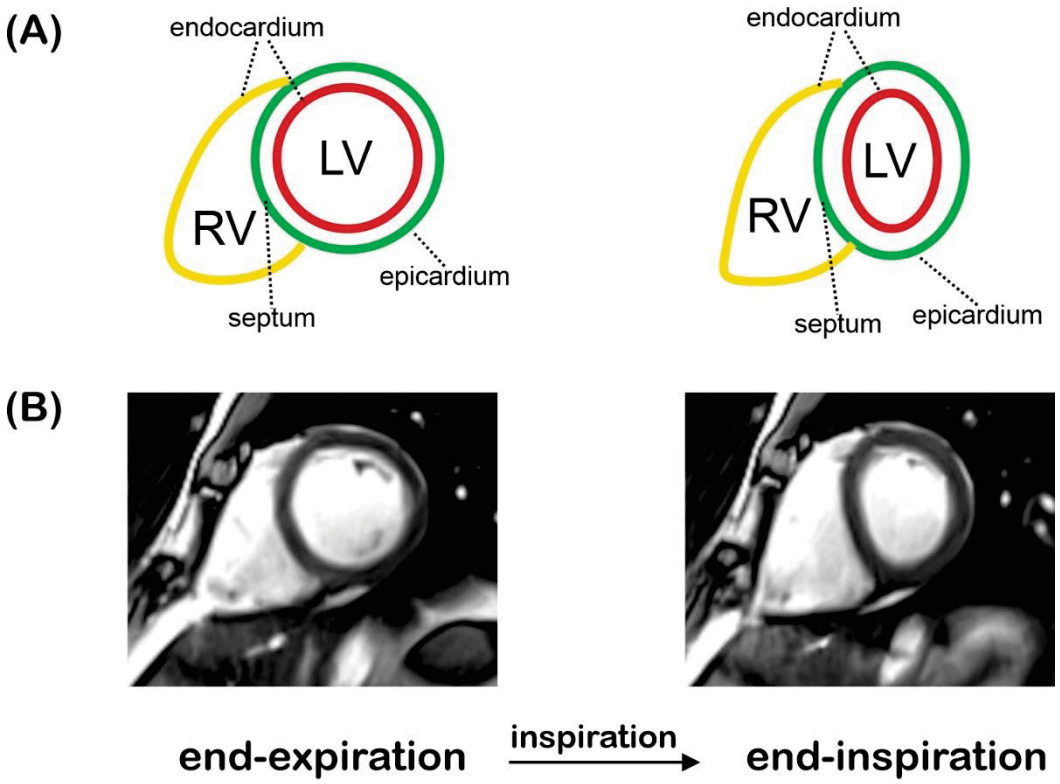

Figure 9. Direct ventricular interactions during inspiration and expiration.

A) Schematized anatomy of the heart with left ventricular epicardial and endocardial and right ventricular endocardial contours during end-diastole. Both ventricles are separated by the flexible septum. With increasing right ventricular (RV) volume in inspiration, the flexible septum shifts to the left ventricle changing the left ventricular (LV) shape.

B) Demonstration of the septal shift during inspiration in cardiac real-time MRI images during end-diastole.

1.5 Registration of respiration during MRI examinations

1.5.1 Conventional methods (respiratory bellows, navigator echoes)

Real-time MRI offers the opportunity to perform data acquisition during free-breathing. This is a major advantage especially for pediatric cardiology. However, free-breathing causes a breath-induced movement of the heart, making an evaluation particularly difficult.

Breath-induced movement is a well-known problem that has been a major challenge for radiology for decades (31, 32). Currently, the problem is most frequently addressed by using respiratory bellows or navigator echoes, registering respiration indirectly (33).

Respiratory bellows are placed on the patient's abdomen, tracing the breathing-induced abdominal and/or thoracal movement during data acquisition **(Figure 10)**. The continuously recorded respiratory bellows signal highly correlates with cardiac displacement during the breathing cycle (33). Thus, it is useful for selecting images from the same breathing phase e.g., end-expiration retrospectively. This technique was used in our experiments to allow a comparison with spirometry.

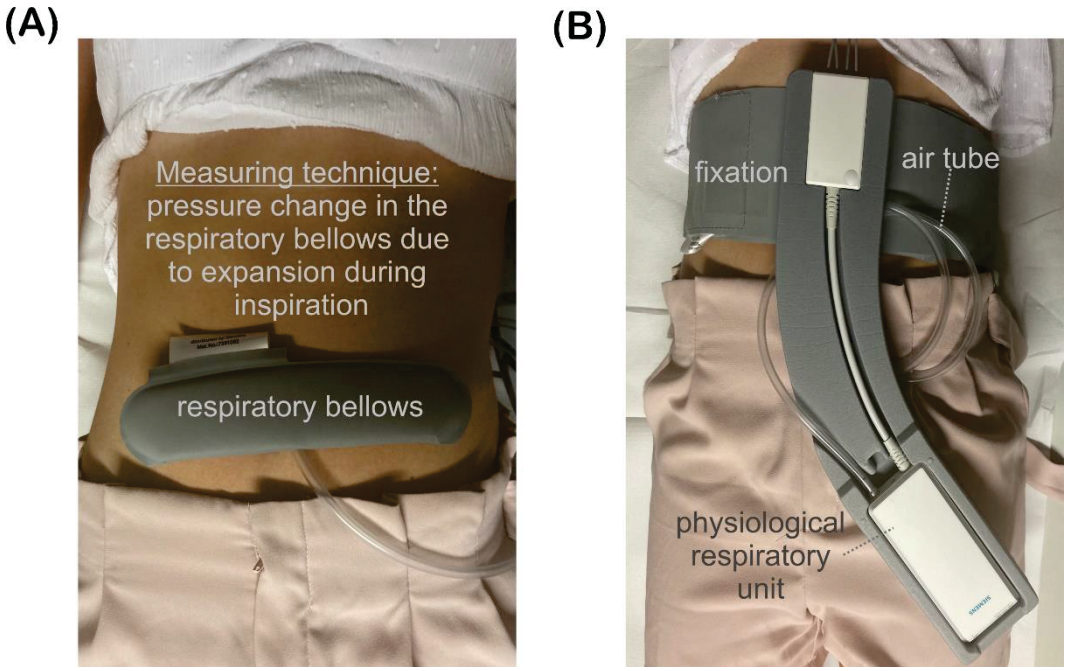

Figure 10. Respiratory bellows.

The respiratory bellows are placed on the subject´s abdomen (A) and individually fixed and connected to the PERU098 Physiological Respiratory Unit from Siemens (B) for the registration of respiratory-induced abdominal movement during real-time MRI data acquisition during free-breathing.

Navigator echoes detect the position of the diaphragm during free-breathing based on a high image contrast between lung and diaphragm **(Figure 11)**. Since the apex cordis is fused with the diaphragm, its movement is highly correlated with the cardiac mean superior-inferior movement during in- and expiration. Therefore, navigator echoes can be used for the determination of certain time points in the breathing cycle predefining the gating window for accepted MR images to be e.g., only in end-expiration (31). For technical reasons, real-time MR imaging could not be combined with navigator echoes.

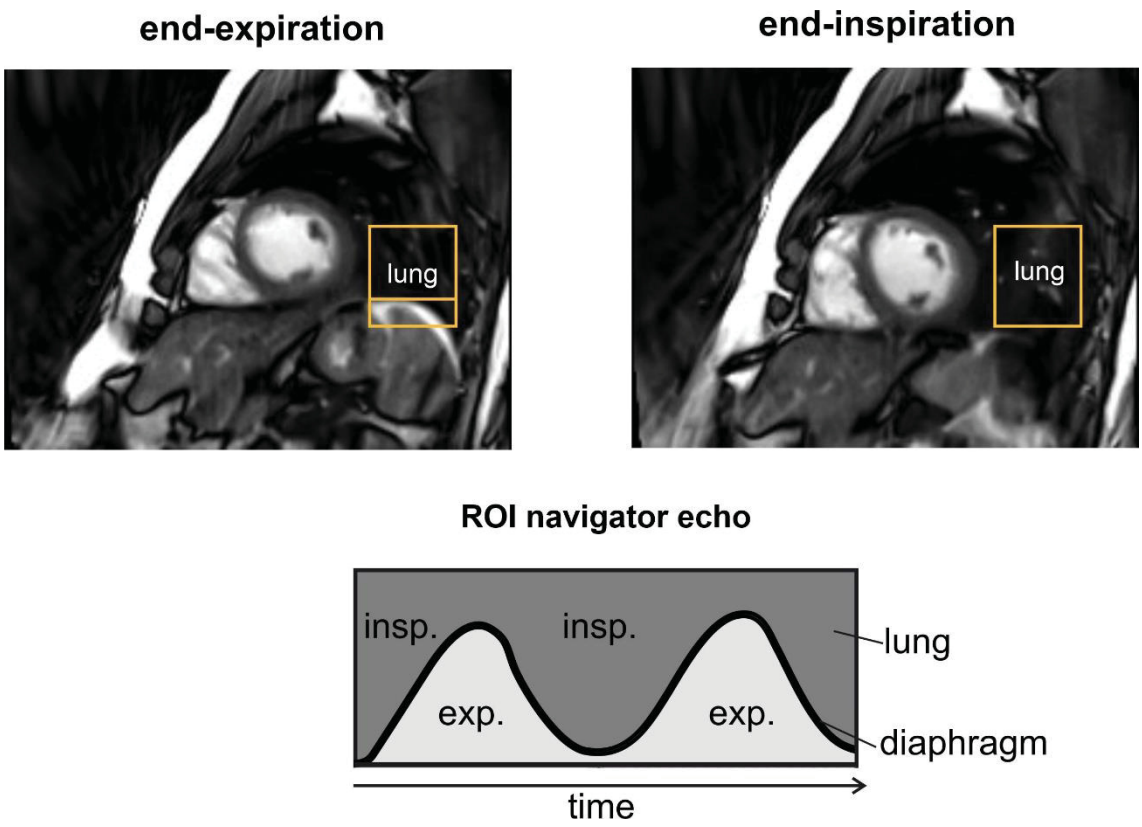

Figure 11. Navigator echoes.

Navigator echoes can be used for the determination of the respiratory phase due to the variation of the diaphragm´s position in the region of interest during in- and expiration (modified from Nehrke K et al. (34)).

Importantly, both methods are only indirect indicators of respiration. Although the problem of breath-induced movement can be improved by the registration of the breathing phase, the quantitative, physiological respiratory influence on cardiac function in the context of heart-lung interactions cannot be addressed quantitatively with these techniques.

1.5.2 MR-compatible spirometry

Eichinger et al. (35) developed a MR-compatible spirometer that allows to perform spirometry during MRI. Since spirometry remains the gold standard for lung volume measurement, it offers the unique possibility for the quantitative evaluation of respiration. Technically, the spirometer consists of the pneumotachograph, that detects pressure differences caused by breathing. Based on Hagen-Poiseuille's law, which implies that the flow velocity in a rigid pipe with laminar flow is proportional to the pressure difference per unit length, the respiratory flow can be calculated. Integration of the flow curve results in the exact lung volume (36) **(Figure 12)**.

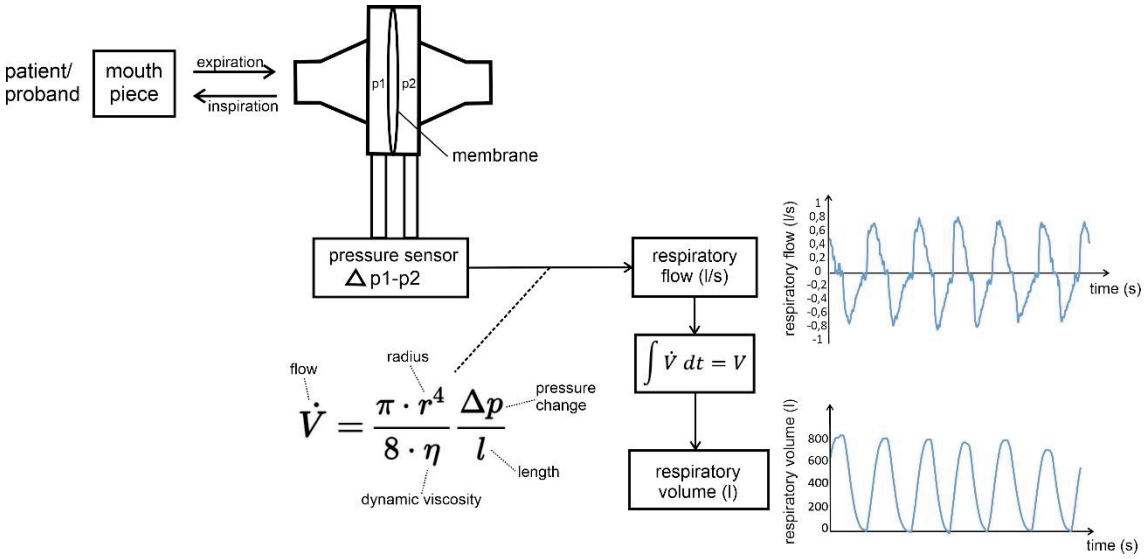

Figure 12. Pneumotachograph.

Basic principle of a pneumotachograph: In- and expiration induces pressure differences detected by a pressure sensor that are used to calculate the respiratory flow based on the Hagen-Poiseuille law. Respiratory volume is calculated from the flow curve.

Previous studies have used spirometry for image stabilization (37).

1.6 Aims of the work

The following feasibility study was designed to test the hypotheses that the combination of real-time volumetry with MR-compatible spirometry

a) is technically feasible,
b) is well-tolerated by subjects,
c) improves motion control during free-breathing and
d) enables the quantification of respiratory-induced cardiac changes (heart-lung interactions) non-invasively.

2 Material and Methods

Parts of the Material and Methods section are published in: Röwer LM, Uelwer T, Hußmann J, et al. Spirometry-based reconstruction of real-time cardiac MRI: Motion control and quantification of heart-lung interactions. Magn Reson Med. 2021;86:2692-2702. https://doi.org/10.1002/mrm.28892

2.1 Data acquisition

2.1.1 Imaging protocol

Adult volunteers (n=4, age 39 ± 14 (24-55) years, two male / two female, body weight 72.5 ± 8.2 kg) were recruited for cardiac MRI studies at a 1.5 Tesla MRI system (MAGNETOM Avanto fit Siemens Healthcare, software version syngo MR E11). Only healthy persons without contraindications for MRI were included. All subjects signed a written declaration of consent based on detailed information and the study was proven by the **ethics committee of the University Hospital Duesseldorf, study number 6176R.**

Conventional cardiac MRI localizers were acquired for the measurement of retrospectively gated four-chamber and two-chamber cine datasets for planning real-time MRI volumetry. Real-time MRI volumetry consisted of a series of cross-sectional real-time MRI movie slices with steady state free precession (SSFP) contrast, field of view: 320mmx320mm, repetition time (TR): 3.7ms, echo time (TE): 1.85ms, 33ms per image covering the left and right ventricle during free-breathing. Dependent on the heart size, 20 slices for three subjects and 14 slices for one subject with 900 phases were acquired, providing 5 respiratory cycles for each slice. The slice thickness was defined as 8 mm and the slices were measured without a distance factor. Imaging of each slice lasted 30 seconds, resulting in a total real-time MRI volumetry time of 10 minutes for 20 slices and 7 minutes for 14 slices **(Figure 13)**.

Simultaneously, the ECG and the abdominal movement from respiratory bellows were registered with Siemens Signal logging VD11a (ECG/RESPIRATORY UNIT, PERU 098 Siemens). Information on the respiratory flow and lung volume were provided by MR-compatible spirometry. **(Figure 13)**.

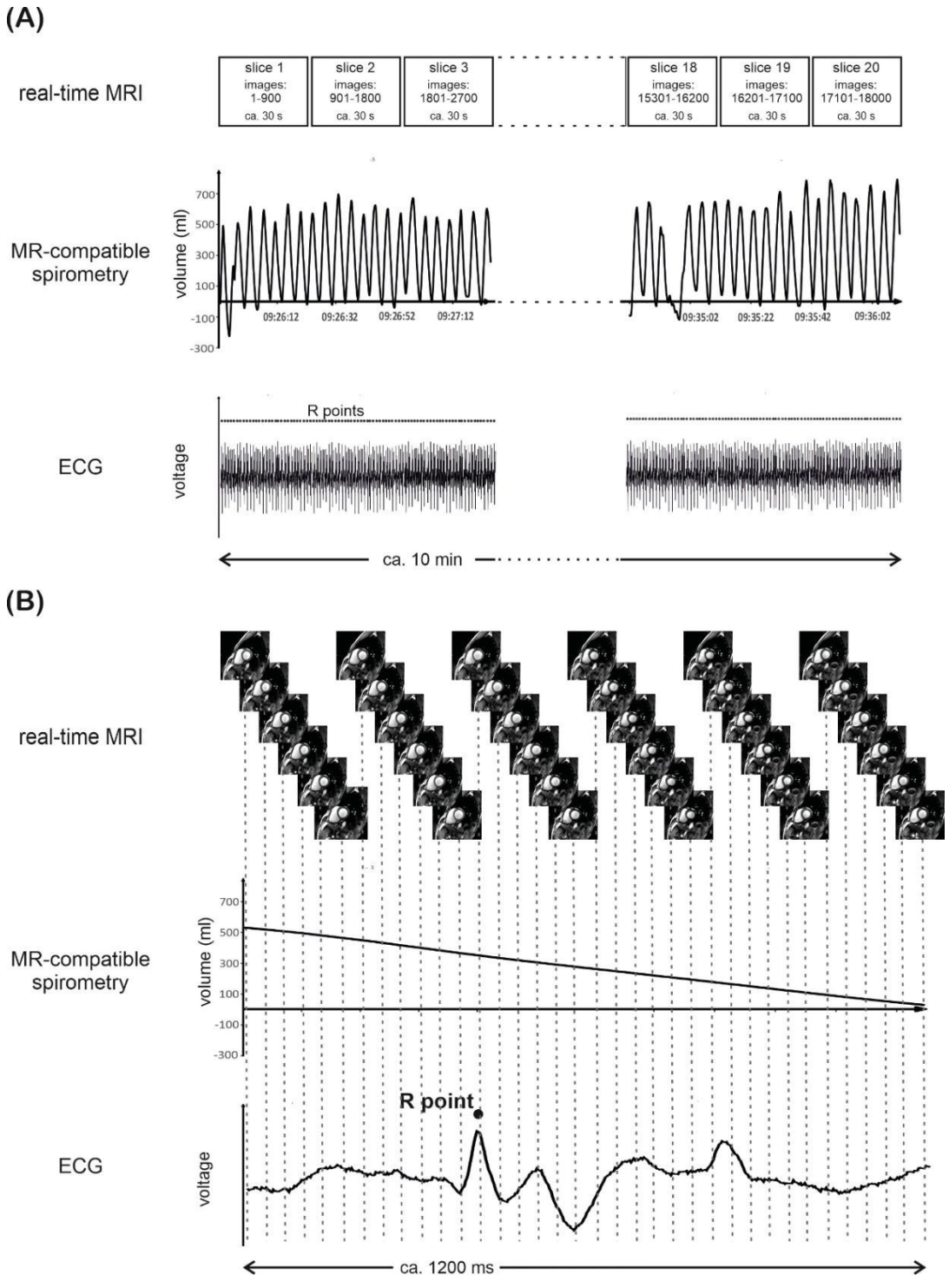

Figure 13. Imaging protocol.

A) Complete protocol: 20 slices were acquired, covering the whole heart with 900 images per slice. MR-compatible spirometry and ECG were registered in parallel.

B) Detailed presentation of 1200ms data acquisition (modified from Röwer LM et al. (38)).

2.1.2 MR-compatible spirometry

The MR-compatible spirometer was developed based on a conventional spirometer (Masterscreen pneumo, VIASYS Healthcare, Hoechberg Germany) with renovations for the use in the MR scanning room. Therefore, the MR-compatible handpiece from the pneumotachograph was freed from all magnetic components and connected via two 7m long pressure tubes (Rauclair®-E; RAU-PVC 8006, internal diameter 3 mm, gauge 1.5 mm) to the original VIASYS healthcare handpiece (Höchberg, Germany) in the control room (35) **(Figure 14 D-F)**. To achieve the highest possible comfort and to avoid the need to hold the handpiece during the MRI examination, the pneumotachograph was connected via a filter (Viaire Microgard® IIC) to a face mask (Hans-Rudolph Mask (7450 Series V2 Mask™)). A custom-made stabilization tool was developed to distribute the weight of the pneumotachograph evenly and to prevent pressure on the face ensuring a comfortable examination situation **(Figure 14 A-C)**.

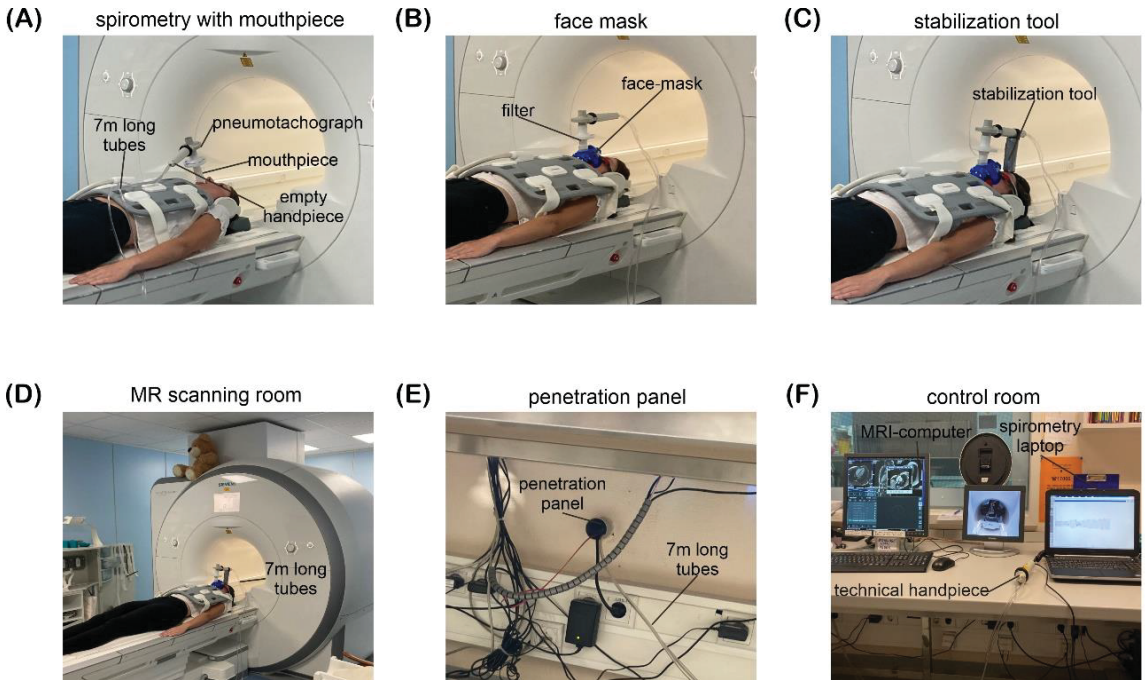

Figure 14. MR-compatible spirometry set-up.

The MR-compatible spirometry set-up was improved by replacing a conventional spirometry mouthpiece (A) with a well-sealed mask (B). A customized stabilization tool was developed to distribute the weight of the pneumotachograph to prevent pressure on the subject's face (C). 7m long pressure tubes connect the pneumotachograph with the empty handpiece in the MR scanning room (D) with the technical handpiece and the spirometry software in the control room (F) through a penetration panel (E).

Following the MRI examination, all subjects were surveyed regarding their anxiety and comfort during the real-time MRI data acquisition with a standardized questionnaire (developed based on Chen S et al. (39) **(Supplement 1)**).

2.2 Binning

The real-time images of each slice of different cardiac cycles were binned into different categories depending on the respiratory information (respiratory flow and lung volume) and ECG information (RR-interval), to enable evaluation of real-time cardiac volumetry during free-breathing **(Figure 15)**.

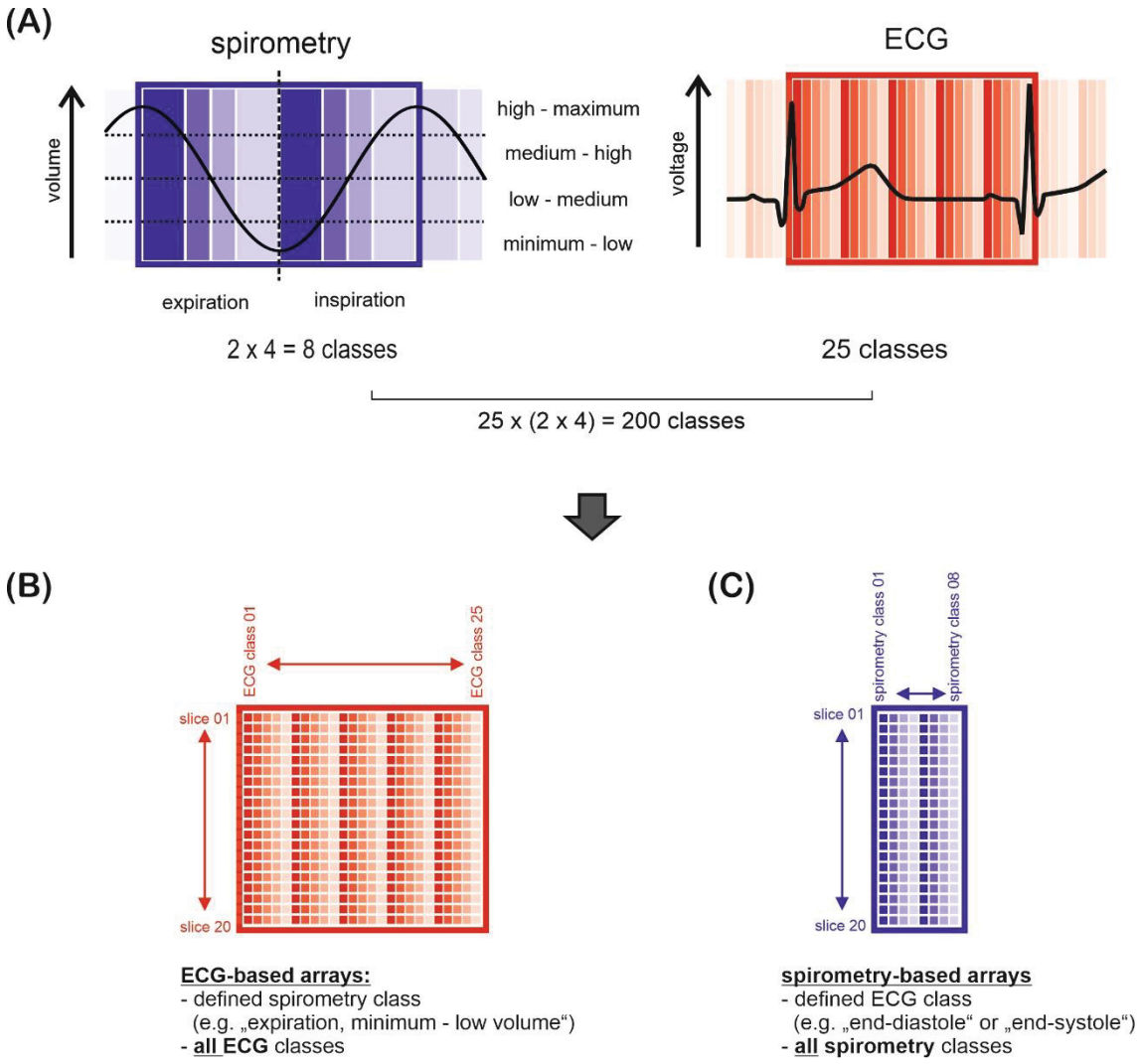

Figure 15. Binning.

A) Images were binned into heart cycles dependent on respiratory information and ECG.

B) Similar to retrospective cine imaging, images were rearranged to a heart cycle for a defined spirometry class.

C) Rearrangement of images for a defined ECG class, but different respiratory classes to visualize effects of respiration on the heart (heart-lung interactions) (modified from Röwer LM et al. (38)).

Binning is the prerequisite for left and right ventricular volumetry analysis based on the arrangement in respiratory dependent heart cycles **(Figure 15B)**.

Additionally, it enables the arrangement and selection of real-time MR images for further analysis focusing on respiratory effects on cardiac function (e.g., heart-lung interactions, eccentricity index) **(Figure 15C)**.

To achieve binning, respiratory flow and lung volume provided by MR-compatible spirometry were written to the dicom tags of the corresponding real-time MR images offline with Python (Python Software Foundation), by adapting published open-source packages (e.g., Numpy (40) and pydicom (41)) **(Figure 16).** ECG-derived information on the time after the R peak had already been included in the dicom tags by the intrinsic MR scanner software (Syngo MR E11, Siemens Healthineers, Erlangen, Germany). Depending on the RR-interval and the respiratory information, real-time MR images were binned into eight respiratory classes, four different lung volume groups each in inspiration and expiration, and 25 cardiac phases (33.5 ± 4.3ms) **(Figures 15A, 16).** The program code that was developed for binning is openly available (https://doi.org/10.5281/zenodo.4899285). Similarly, real-time MRI images were binned with respiratory bellows data instead of spirometry data.

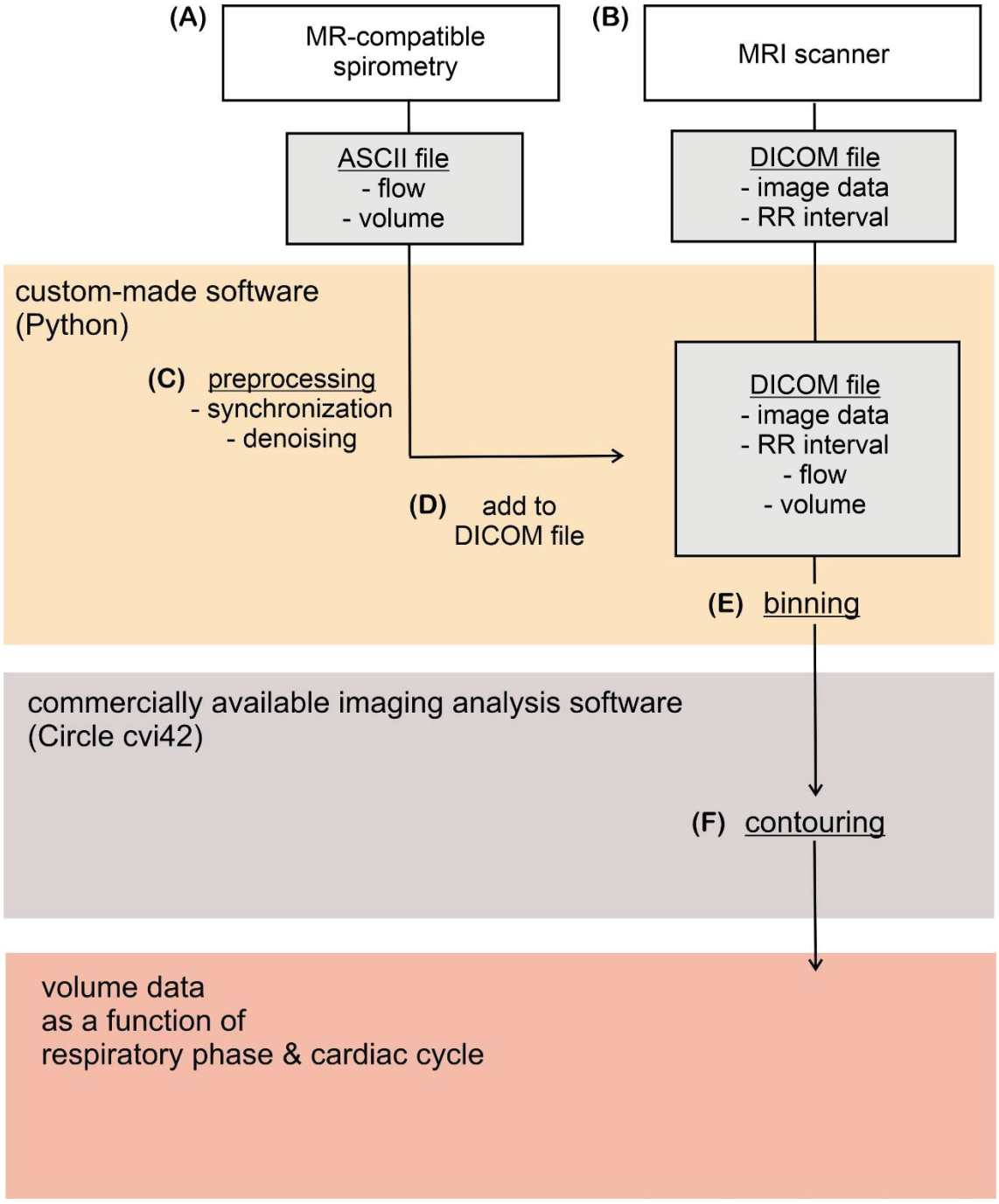

Figure 16. Data preprocessing and binning.

MR-compatible spirometry derived respiratory flow and lung volume (A) and real-time MR-images including ECG data (RR-interval) (B) were imported to Python. After preprocessing (C), spirometry volume and respiratory flow were added to the dicom tags of the corresponding MR-images (D). Depending on the spirometry volume, the respiratory flow and the information on the time after the R-peak, the images were binned in respiratory classes (E) and exported from Python for further evaluation in a commercially available analysis software (F).

The typical tidal volume and heart rate from each subject was used to optimize binning, especially regarding minimizing the number of empty classes. In the case of unfilled bins, images from the following ECG classes were used for filling and the images were excluded from the evaluation. For bins where multiple images were available, the one closest to the median of the lung volume of the corresponding spirometry class was chosen.

2.3 Data analysis

After respiratory-dependent binning and rearrangement to heart cycles, the real-time MR volumetry images were analyzed focusing on three different aspects:

1. Evaluation regarding an achieved benefit for motion control
2. Respiratory influence on the left ventricular eccentricity index
3. Respiratory influence on the right and left ventricular volume

The left ventricular eccentricity index and the respiratory effect on the right and left ventricular volumetry were evaluated with a commercial cardiac MR software (cvi42; Release 5.10.1.(1241); Circle Cardiovascular Imaging Inc. Calgary, Canada).

2.3.1 Motion control

Motion control is a prerequisite for a high-quality analysis both by qualitative, visual assessment (“eyeballing”), but also using an automated evaluation. A midventricular slice was selected for the characterization of cardiac movement and the quantification of motion control in all subjects and all respiratory categories. To achieve this, the cranial and caudal junction of the interventricular septum with the right ventricle were determined manually. The displacement of the midpoint between these two points served as the basis for the analysis of anterior(-right)-to-posterior(-left), superior(-left-anterior)-to-inferior(-right-posterior) displacement and rotation of the heart during the arranged heart cycles **(Figure 17)**. The evaluation of motion control in eight cardiac cycles, binned with the respiratory information from MR-compatible spirometry and ECG, were compared to eight heart cycles solely sorted by ECG and eight heart cycles sorted by data from respiratory bellows and ECG from the same midventricular slice for all subjects.

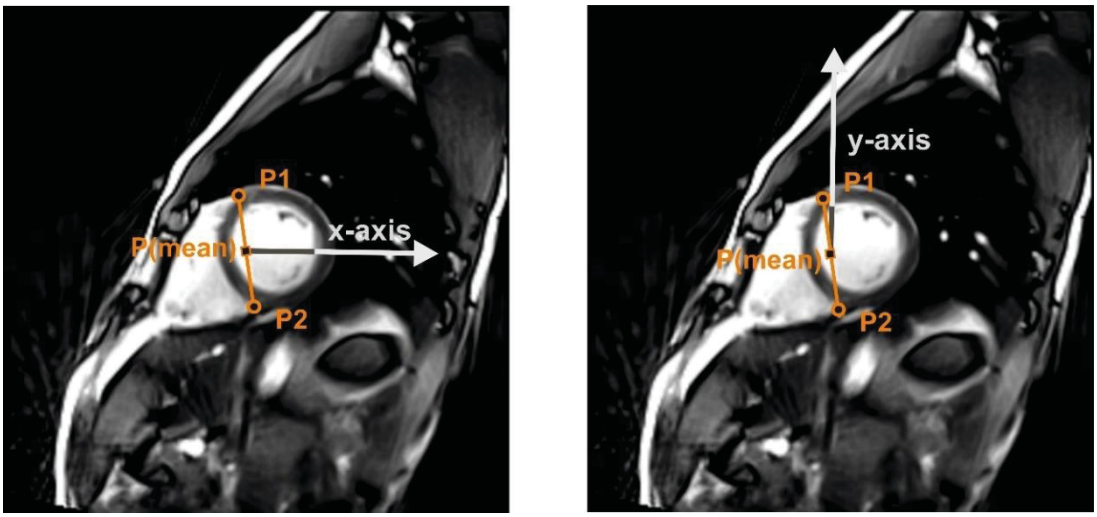

Figure 17. Evaluation of motion control.

P(mean) was defined as midpoint between the cranial (P1) and caudal (P2) junction of the interventricular septum with the right ventricle and used as reference point for the analysis of motion control (modified from Röwer LM et al. (38)).

2.3.2 Left ventricular eccentricity index

The left ventricular eccentricity index was determined for all end-diastolic and end-systolic phases of a midventricular slice for all spirometry-dependent binned heart cycles from all volunteers. Therefore, the series overview module from Circle cardiac MRI software cvi 42 was used to draw the horizontal diameter perpendicular to the septum and the vertical diameter parallel to the septum separately for the endocardial and epicardial contours **(Figure 18)**. Subsequently, the left ventricular eccentricity indices were calculated:

End-diastole:

EId (endocardial) = D2/D1 (endocardial)**,** EId (epicardial) = D2/D1 (epicardial)

End-systole:

EIs (endocardial) = S2/S1 (endocardial)**,** EIs (epicardial) = S2/S1 (epicardial)

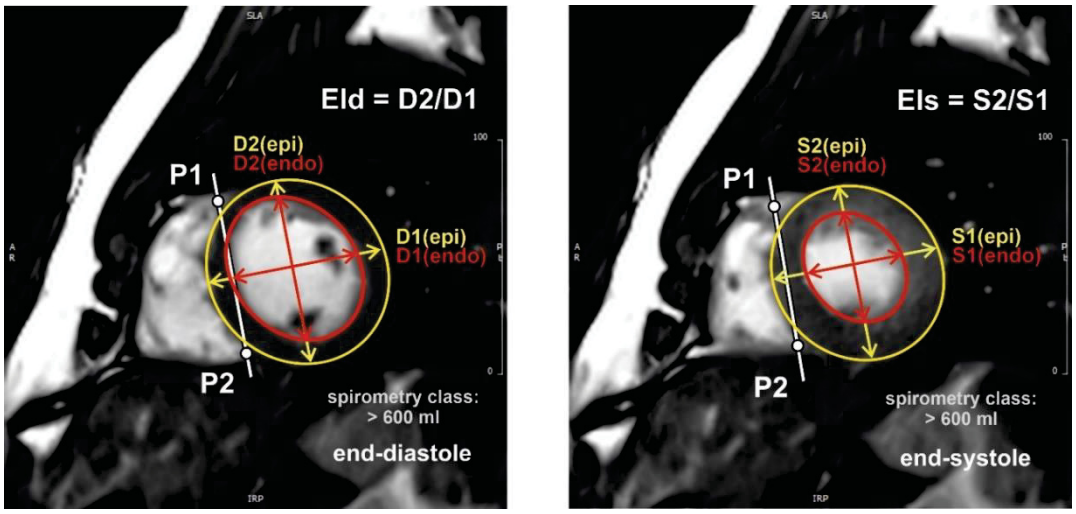

Figure 18. Evaluation of LV eccentricity index.

The left ventricular eccentricity index was calculated for end-diastolic and end-systolic phases of a midventricular slice for the endocardial (red) and epicardial (yellow) border. The eccentricity index is defined as the ratio of the axis parallel to the interventricular septum (D2, S2) to the perpendicular axis (D1, S1) (modified from Röwer LM et al. (38)).

2.3.3 Right and left ventricular volumetry

The calculation of right and left ventricular volumes was performed for all eight respiratory categories with the Short3D module of the cardiac MRI software cvi 42 (Circle Cardiovascular Imaging Co.) by automatically contouring the left ventricular epicardial and endocardial and right ventricular endocardial borders.

Thereafter, manual corrections were performed applying current recommendations on image analysis and a real-time MRI contoured dataset for reference (42, 43, 44, 45), **(Figure 19)**, **(Video link to the supplemental digital content:** https://onlinelibrary.wiley.com/action/downloadSupplement?doi=10.1002%2Fmrm.28892&file=mrm28892-sup-0001-VideoS1.mp4**)**.

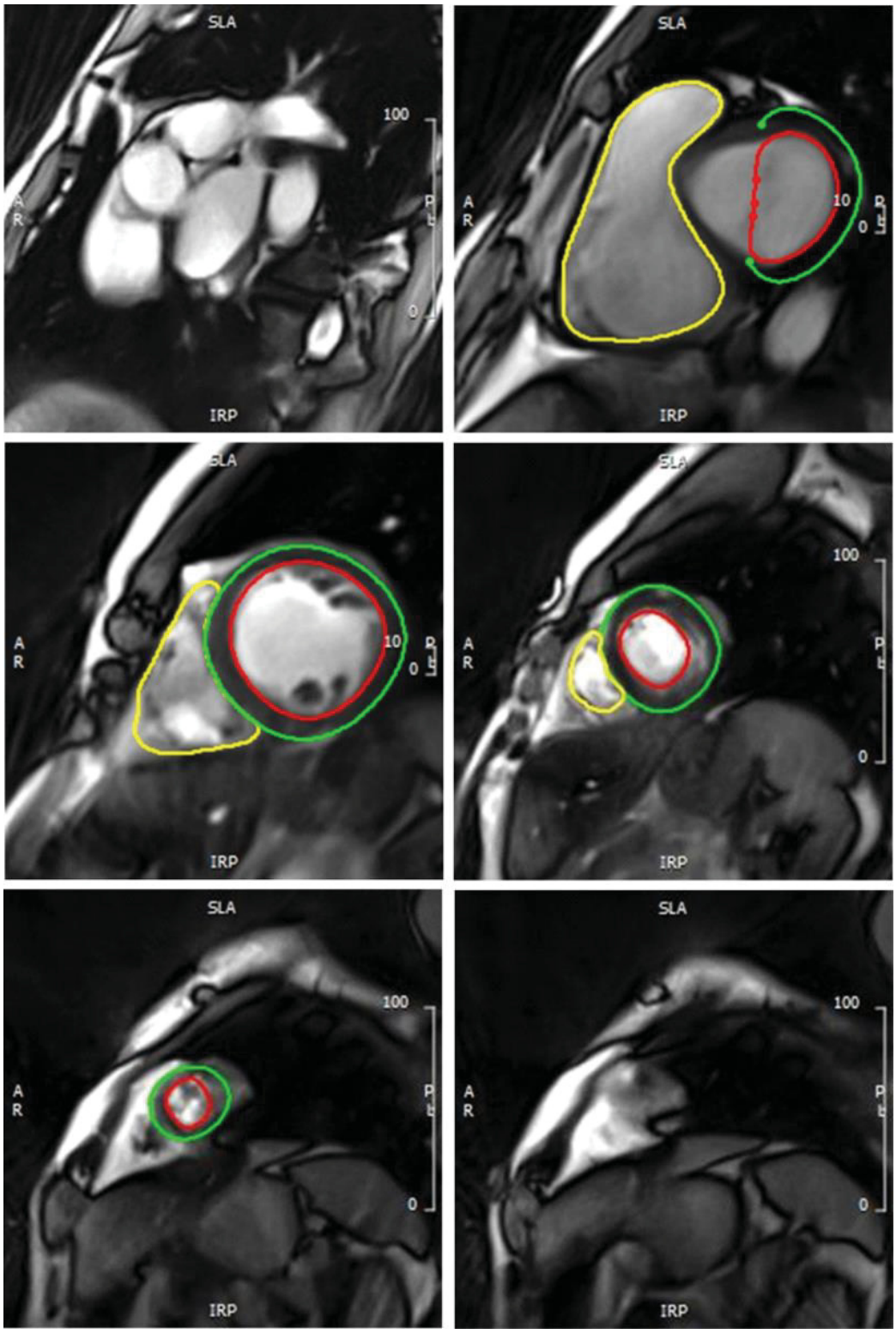

Figure 19. Contouring reference images.

Reference images served as basis for manual contour corrections for the left ventricular epicardial (green) and endocardial (red) border as well as right ventricular endocardial border (yellow) (modified from Röwer LM et al. (38)).

As recommended by current cardiac MRI guidelines and because detection was unreliable, papillary muscles were included in the ventricular volume (42, 45).

The end-systolic and end-diastolic phases were defined separately for the left and right ventricle as phases with the smallest (end-systolic) and largest (end-diastolic) blood volume of the corresponding ventricle (43).

The basal slice of the left ventricle was defined as the first end-diastolic slice with more than 50% myocardium surrounding the blood volume **(Figure 20A)**. The right ventricular basal slice was defined as the first slice that was completely apical of the tricuspid valve and consequently part of the right ventricle. The position of the slice was evaluated with the help of the multiplanar cross-referencing tool from Circle cvi 42 demonstrating the position of the slice in the four-chamber view (44) **(Figure 20B)**.

Apical slices of the ventricles were evaluated separately for the left and right ventricle and determined as most apical slice of the stack with visible right or left ventricular cavity (43) **(Figure 20C)**.

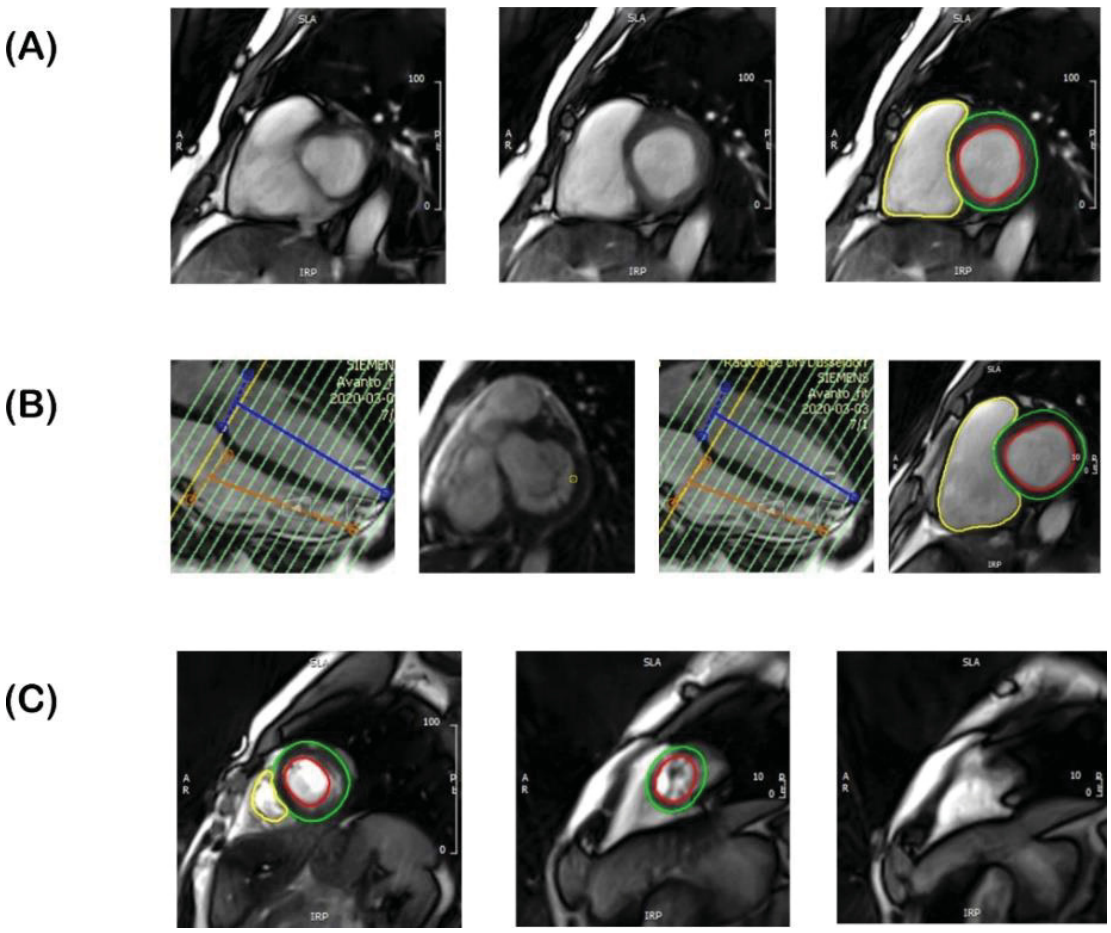

Figure 20. Definition of the basal and apical slice.

A) Left ventricular basal slice is included and contoured when 50% of the circumference was ventricular myocardium (slice in the middle). The slice on the left was excluded because less than 50% of the circumference was ventricular myocardium.

B) Right ventricular basal slice is included when the yellow line in cross-referencing showed that the slice is part of the ventricle (right part) and excluded when cross-referencing showed that it is part of the atrium (left part)

C) The apical slice is contoured when containing visible right and/or left ventricular cavity (modified from Röwer LM et al. (38)).

2.3.4 Frank-Starling mechanism

Based on the left and right ventricular volumetry, the Frank-Starling relationship between end-diastolic volume and stroke volume was calculated **(Figure 21)**.

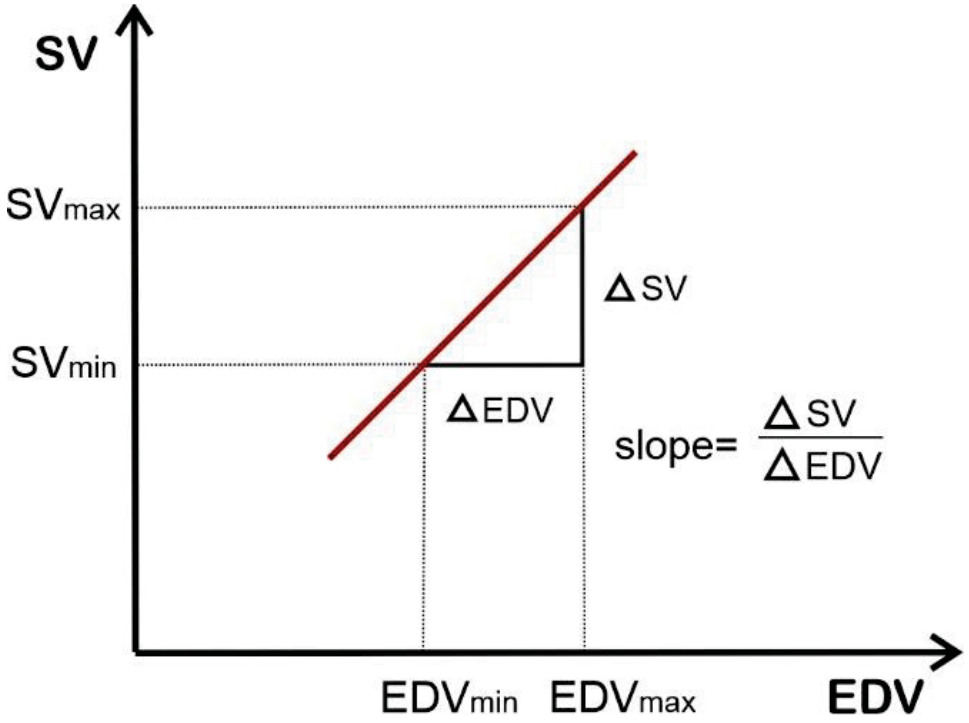

Figure 21. Frank-starling curve slope calculation.

The slope of the Frank-Starling curve was calculated from the difference between maximum and minimum of the stroke volume divided by the difference between the maximum and minimum of the end-diastolic volume.

2.4 Statistical analysis

SPSS (IBM Corp. Released 2017, IBM SPSS Statistics for Windows, Version 25.0. Armonk, NY: IBM Corp.) was used to calculate the statistical analysis for the motion control results, results on ventricular volumetry and the left ventricular eccentricity index.

First, the motion control data were checked for normal distribution using the Shapiro-Wilk test. Due to non-normally distributed data, the further statistical evaluation was performed with the non-parametric Wilcoxon matched pair test and the Kruskal-Wallis test.

The relationship between the left and right ventricular volumetry and the corresponding lung volume and respiratory flow was tested for a statistically significant correlation using linear regression. In addition, linear regression analysis was calculated to assess the effect of the spirometry volume on the end-diastolic and end-systolic left ventricular eccentricity index.

Test results with $p < 0.05$ were considered statistically significant.

3 Results

Parts of the Results section are published in: Röwer LM, Uelwer T, Hußmann J, et al. Spirometry-based reconstruction of real-time cardiac MRI: Motion control and quantification of heart-lung interactions. Magn Reson Med. 2021;86:2692-2702. https://doi.org/10.1002/mrm.28892

3.1 MR-compatible spirometry

MR-compatible spirometry showed that all subjects breathed calmly and evenly during the real-time MRI data acquisition. The mean respiratory rate was 13.45 ± 1.44 per minute with a tidal volume of 9.86 ± 3.75 ml/kg (end-inspiratory volume 9.8 ± 3.7 ml/kg; n=4) resulting in a respiratory minute volume of 125.6 ± 38.3 ml/kg/min.

3.2 Comfort survey

The results of the comfort survey **(Table 1)** proved that the subjects' degree of anxiety during cardiac real-time MRI was low and hardly influenced by additional spirometry. Overall comfort with connected spirometry was still high but lower than without spirometry (5.75 ± 0.43 vs. 7.75 ± 0.43; numeric rating scale 1 = low comfort, 10 = high comfort).

However, comfort reduction by spirometry was lower (3.25 ± 0.83; n=4) than the reduction of comfort by other factors (climate (heat, draft or cold): 4.50 ± 2.29, duration of the scan: 3.75 ± 2.49, back pain: 3.50 ± 2.60; acoustic noise: 3.50 ± 1.12; n=4 for all).

test item	specification	subject				mean ± standard deviation
		01	02	03	04	
overall comfort (1 = low, 10 = high)	with mask connected to spirometry	5	6	6	6	**5.8 ± 0.4**
	with mask but not connected to spirometry	6	7	7	7	**6.8 ± 0.4**
	without mask/spirometry	7	8	8	8	**7.8 ± 0.4**
anxiety (1 = low, 10 = high)	with mask connected to spirometry	1	3	2	3	**2.2 ± 0.8**
	with mask but not connected to spirometry	1	2	2	3	**2.0 ± 0.7**
	without mask/spirometry	1	2	2	3	**2.0 ± 0.7**
comfort restriction (1 = not at all, 10 = very much)	duration of the scan	8	3	2	2	**3.8 ± 2.5**
	acoustic noise	2	3	5	4	**3.5 ± 1.1**
	chest coil	3	2	1	1	**1.8 ± 0.8**
	neck and or back pain	7	5	1	1	**3.5 ± 2.6**
	peripheral nerve stimulation	1	2	1	1	**1.2 ± 0.4**
	climate (heat, draft, cold)	3	2	8	5	**4.5 ± 2.3**
	spirometry	4	4	2	3	**3.2 ± 0.8**
	claustrophobia	3	2	2	2	**2.2 ± 0.4**
	not being allowed to move	2	7	7	4	**5.0 ± 2.1**
	unspecific fear/anxiety	2	2	1	2	**1.8 ± 0.4**

Table 1. Comfort survey results.

Detailed presentation of the comfort survey results for all subjects (modified from Röwer LM et al. (38)).

3.3 Binning

Binning would be optimal if exactly one image was available for each category. In this case, for hearts with 20 slices (20 slices x 25 ECG phases x 8 spirometry classes) 4000 images would be sufficient, for hearts with 14 slices (14 slices x 25 ECG classes x 8 spirometry classes) a number of 2800 images would be necessary **(Figure 22)**.

The distribution of the images among the ECG classes was uniform and was additionally optimized for each subject by a class definition based on the mean RR-interval. Thus, only a small proportion of images in the ECG classes that exceeded the mean RR-interval had to be excluded **(Figure 22 A, B (n=1), Table 2 (n=4))**. The very even distribution among ECG classes resulted in a high number of available images per ECG class **(Figure 22 C (n=1), Table 2 (n=4)).**

In contrast, the distribution among spirometry classes was uneven **(Figure 22 D, E (n=1), Table 3 (n=4))**. Significantly more images were available in the high and low respiratory volume classes for inspiration and expiration (68.9% of all images after excluding RR intervals above the mean RR interval), whereas significantly less images were available in the middle respiratory classes (31.1%). This resulted in a higher number of filled classes in the high and low spirometry categories of 99.5% and a significantly lower percentage of filled classes in the middle spirometry classes (93%) **(Figure 22 F (n=1), Table 3 (n=4))**.

To have a sufficiently high number of filled classes available in the middle respiratory categories despite the uneven lung volume distribution and to achieve the best possible ratio of overfilled to empty bins, it was necessary to extend the acquisition time and to increase the optimal total number of images to 4000 (for 20 slices) and to 2800 (for 14 slices), respectively.

Acquisition of 138-199 images per combined respiratory and ECG class corresponding to a percentage of 186-269% of the minimum required images, allowed filling the combined categories with 80-84% for 9.5% of all classes, with 85-89% for 23.8%, with 36.5% for 90-95% and a nearly complete filling with 95-99% of all classes with 30.2%.

When 200-299 images, corresponding to 270-400% of the minimum number of required images were available, 2.1% of the classes could be filled with 85-89%, 10.6% with 90-94%, 63.8% with 95-99% and 23.4% of all classes could be filled completely.

With 400-540% of the minimum number of required images per class, corresponding to 300-399 images, all classes could be filled by more than 90%. 5.6% of the classes

showed a filling of 90-94%, 27.8% had a filling of 95-99% and 66.7% of the classes were filled completely.

400-486 available images (i.e., 540-650% of the minimum number required) resulted in a fill of 95-99% for 23.7% of all classes. 76.3% could then be filled completely.

As soon as more than 486 images, corresponding to 650% of the minimum necessary images, were available, all classes were always filled completely for all subjects.

The defined data acquisition of 900 images per slice results in a total number of 68000 real-time images for all subjects together, corresponding to 4.6 times the total number of bins to be filled, and serves as a prerequisite for a very low number of empty classes of only about 4% **(Tables 2,3)**.

In conclusion, the number of images should be ~4-5 times the number of bins to obtain good results.

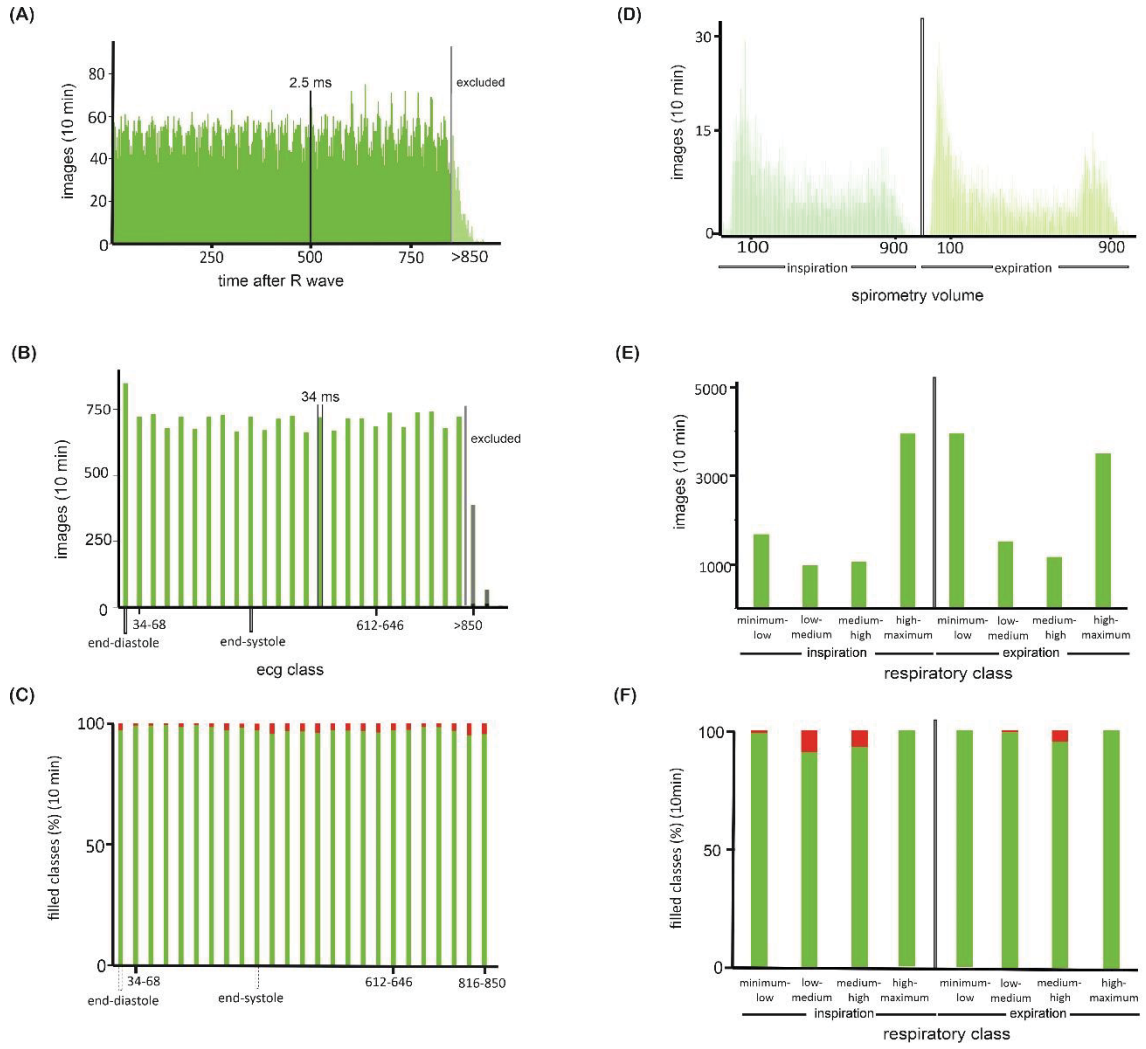

Figure 22. Distribution.

Among the ECG classes there was a very even distribution of images. Accordingly, all classes were filled evenly and without empty classes (A-C). In contrast, the images of the spirometry classes were unevenly distributed. In the high and low respiratory classes there were many images, and almost all classes could be filled. In the middle respiratory categories, fewer images were available, so that not all of them could be filled completely (D-F) (modified from Röwer LM. et al. (38)).

ECG phase	subject 1			subject 2			subject 3			subject 4			sum	
	time (ms)	number of images	filled phases (%) *	time (ms)	number of images	filled phases (%) *	time (ms)	number of images	filled phases (%) *	time (ms)	number of images	filled phases (%) **	number of images	filled phases (%) ***
1	0-40	899	95.6	0-34	849	96.9	0-32	613	93.8	0-28	514	97.3	2865	95.8
2	41-80	693	95.6	35-68	722	98.8	33-64	564	93.8	29-56	474	96.4	2453	96.1
3	81-120	665	96.3	69-102	731	98.8	65-96	614	96.3	57-84	466	96.4	2476	97.0
4	121-160	695	95.0	102-136	679	99.4	97-128	609	95.0	85-112	515	98.2	2498	96.8
5	161-200	660	96.9	137-170	721	97.5	129-160	616	95.0	113-140	460	97.3	2457	96.6
6	201-240	669	96.9	171-204	676	99.4	161-192	618	95.0	141-168	459	98.2	2422	97.3
7	241-280	691	96.3	205-238	721	97.5	193-224	577	95.0	169-196	461	96.4	2450	96.3
8	281-320	661	98.1	239-272	729	96.9	225-256	615	95.6	197-224	473	97.3	2478	96.5
9	321-360	692	98.8	273-306	666	97.5	257-288	615	95.6	225-252	510	99.1	2483	97.5
10	361-400	653	97.5	307-340	721	96.9	289-320	609	96.3	253-280	460	99.1	2443	97.6
11	401-440	668	98.1	341-374	671	95.0	321-352	604	95.6	281-308	466	97.3	2409	96.3
12	441-480	680	96.3	375-408	714	96.3	353-384	574	94.4	309-336	459	95.5	2427	96.1
13	481-520	657	96.3	409-442	725	96.6	385-416	607	96.9	337-364	446	98.2	2435	96.6
14	521-560	687	95.6	443-476	663	95.6	417-448	603	96.3	365-392	507	98.2	2460	96.5
15	561-600	647	97.5	477-510	720	96.9	449-480	601	96.9	393-420	473	94.6	2441	96.1
16	601-640	681	96.9	511-544	668	96.3	481-512	609	96.9	421-448	457	97.3	2415	97.0
17	641-680	695	96.9	545-578	716	96.3	513-544	550	95.6	449-476	465	98.2	2426	96.6
18	681-720	691	96.3	579-612	715	95.6	545-576	597	95.6	477-504	449	95.5	2452	95.9
19	721-760	685	96.3	613-646	686	96.9	578-608	604	96.9	505-532	489	98.2	2464	97.0
20	761-800	653	96.9	647-680	737	96.9	609-640	626	99.4	533-560	457	96.4	2473	97.5
21	801-840	658	95.0	681-714	683	97.5	641-672	624	98.1	561-588	464	97.3	2429	97.0
22	841-880	655	94.4	715-748	739	97.5	673-704	569	96.9	589-616	459	96.4	2422	96.3
23	881-920	651	93.8	749-782	741	96.3	705-736	584	95.0	617-644	470	96.4	2446	95.3
24	921-960	624	92.5	783-816	679	94.4	737-768	507	90.6	645-672	449	92.9	2259	92.6
25	961-1000	550	90.6	817-850	722	95.0	769-800	422	85.6	672-700	368	97.3	2062	91.7
mean ± sd		**674 ± 53**	**96.0 ± 1.8**		**712 ± 38**	**96.9 ± 1.3**		**589 ± 43**	**95.3 ± 2.5**		**467 ± 28**	**97.0 ± 1.4**	**2442 ± 122**	**96.2 ± 1.3**
binned		**16850 (93.6%)**			**17794 (98.9%)**			**14731 (81.8%)**			**11670 (83.4%)**		**61045 (89.8%)**	
excluded		**1150 (6.4%)**			**206 (1.1%)**			**3269 (18.1%)**			**2330 (16.6%)**		**6955 (10.2%)**	
acquired		**18000**			**18000**			**18000**			**14000**		**68000**	

* phases are defined as all corresponding categories in the defined ECG phase (8 respiratory classes x 20 slices), ** phases are defined as all corresponding categories in the defined ECG phase (8 respiratory classes x 14 slices)
*** phases are defined as sum of all corresponding categories in the defined ECG phases for all subjects; end-diastolic (ECG phase 1) and end-systolic ECG classes (ECG phase 11, resp. 12) are highlighted by light gray

Table 2. Distribution of MR images among the ECG classes.

The distribution among the ECG classes was even, resulting in a high percentage of filled classes (modified from Röwer LM et al. (38)).

respiratory class		subject 1			subject 2			subject 3			subject 4			sum	
spirometry volume	respiratory phase	volume (ml/kg)	number of images	filled classes (%) *	volume (ml/kg)	number of images	filled classes (%) *	volume (ml/kg)	number of images	filled classes (%) *	volume (ml/kg)	number of images	filled classes (%) **	number of images	filled classes (%) ***
minimum-low	inspiration	<2.1	2404	99.6	<2.3	1679	98.8	<3.0	2193	100	<1.1	1262	100.0	7538	99.5
low-medium		2.1-4.2	1338	87.6	2.3-4.7	979	90.4	3.0-6.0	988	89.9	1.1-2.2	845	95.0	4150	90.0
medium-high		4.2-6.2	1438	87.4	4.7-7.0	1052	92.4	6.0-9.0	976	87.4	2.2-3.2	984	96.0	4450	99.5
high-maximum		>6.2	2733	99.6	>7.0	3949	100	>9.0	2582	99.4	>3.2	2278	99.0	11542	99.7
minimum-low	expiration	<2.1	3281	100.0	<2.3	3952	100	<3.0	3272	100	<1.1	1694	100.0	12199	100.0
low-medium		2.1-4.2	1728	98.4	2.3-4.7	1519	98.8	3.0-6.0	1334	95.6	1.1-2.2	1055	97.6	5636	97.4
medium-high		4.2-6.2	1535	95.6	4.7-7.0	1164	94.8	6.0-9.0	1032	92.2	2.2-3.2	1012	97.2	4743	94.5
high-maximum		>6.2	2393	99.8	>7.0	3500	100	>9.0	2354	97.8	>3.2	2540	98.6	10787	99.0
mean ± sd			**2106 ± 657**	**96 ± 5.1**		**2224 ± 1247**	**96.6 ± 3.6**		**1841 ± 819**	**95.3± 4.6**		**1459 ± 602**	**98 ± 1.7**	**7631 ± 3175**	**96 ± 3.9**
binned images			**16850 (93.6%)**			**17794 (98.9%)**			**14731 (81.8%)**			**11670 (83.4%)**		**61045 (89.8%)**	
excluded images			**1150 (6.4%)**			**206 (1.1%)**			**3269 (18.1%)**			**2330 (16.6%)**		**6955 (10.2%)**	
acquired images			**18000**			**18000**			**18000**			**14000**		**68000**	

* classes are defined as all corresponding categories in the defined respiratory class (25 ECG classes x 20 slices), ** classes are defined as all corresponding categories in the defined respiratory class (25 ECG classes x 14 slices), *** classes are defined as sum of all corresponding categories in the defined respiratory classes (n=4)

Table 3. Distribution of MR images among the spirometry classes.

MR images were unevenly distributed among the spirometry classes with a higher number of images in the lowest and highest respiratory class and a lower number of images in the medium respiratory classes, resulting in a lower percentage of filled classes in the medium spirometry categories (modified from Röwer LM et al. (38)).

3.4 Motion control

Already the visual inspection of the cardiac cycles sorted by ECG and spirometry, by ECG and respiratory bellows and solely ECG sorted heart cycles showed significant differences related to motion control **(Video link to the supplemental digital content:** https://onlinelibrary.wiley.com/action/downloadSupplement?doi=10.1002%2Fmrm.28892&file=mrm28892-sup-0002-VideoS2.mp4**).**

Cardiac cycles that were created solely based on the ECG information (time after the R-wave) without considering the respiratory information resulted in blurred sequences that could hardly be assessed visually. In contrast, simultaneous consideration of respiratory information via either MR-compatible spirometry or respiratory bellows data achieved high image stability of the contiguous images in the defined respiratory classes. The resulting motion control allows significant advantages for further analysis of the real-time volumetry data even when viewed purely visually.

Quantitative analysis of motion within cardiac cycles as compared to a defined reference point in a midventricular slice from all subjects confirmed the results of visual observation. The cardiac cycles whose binning additionally considered the respiratory information resulted in significantly less motion compared with the cardiac cycles considered only on the ECG information **(Tables 4-7 for details, Figure 23 A-J))**. Using the respiratory information of the respiratory bellows as well as spirometry, motion between successive images of a cardiac cycle could be reduced to less than ~1mm **(Tables 4-7, Figure 23 C-J)**. These results were confirmed for all subjects and all spirometry and respiratory bellows categories.

Analysis of the motion in the different respiratory classes allowed quantification of the breath-induced motion of the heart. The main movement of the heart during a respiratory cycle was in the direction of the y-axis (i.e., from superior(-left-anterior) to inferior(right-posterior)), whereas the movement in the direction of the x-axis (anterior(-right) to posterior(-left)) was much less pronounced. Rotational movement was minimal **(Tables 4-7, Figure 23 C-J)**.

Since the results of the four subjects hardly differed and the Kruskal-Wallis test did not confirm a significant difference, the subsequent evaluation of motion control was calculated for all subjects together.

There was a reduction to 29 ± 28% for motion along the y-axis and a reduction to 44 ± 44% for motion along the x-axis in the cardiac cycles that additionally accounted for respiratory information compared with the cardiac cycles solely sorted by ECG.

In summary, the overall mean motion between subsequent phases was reduced to 34 ± 26% in the cardiac cycles sorted by ECG and spirometry as compared to solely ECG sorted heart cycles. Non-parametric Wilcoxon matched pair test achieved significant results for the motion control achieved in the x- and y-axis direction as well as for the total movement reduction in the respiratory sorted cardiac cycles for all subjects **(Tables 4-7)**.

Since rotation between images within a cardiac cycle was negligible, no further significant reduction could be achieved with the aid of respiratory binning **(Tables 4-7)**.

respiratory volume	respiratory phase	number of phases (%)	mean spirometry volume (ml)	mean position (mm) and angulation (°)			mean displacement (mm) and rotation (°)			
				x-axis	y-axis	angulation	x-axis	y-axis	total	rotation
spirometry-based classification										
<150 ml	**inspiration**	25 (100%)	-20 ± 29	0.00 ± 0.71	0.00 ± 0.58	5.60 ± 1.54	0.38 ± 0.32	0.46 ± 0.41	0.69 ± 0.40	0.60 ± 0.57
	expiration	25 (100%)	-28 ± 26	1.44 ± 1.69	-2.02 ± 0.88	6.14 ± 1.93	0.79 ± 0.99	0.61 ± 0.49	1.13 ± 0.97	1.10 ± 1.25
150-300 ml	**inspiration**	22 (88%)	191 ± 30	-0.33 ± 1.14	-1.69 ± 0.93	5.36 ± 1.78	0.75 ± 0.61	0.64 ± 0.38	1.05 ± 0,62	4.37 ± 1.90
	expiration	25 (100%)	219 ± 24	3.26 ± 0.89	-5.89 ± 0.81	5.14 ± 1.65	0.47 ± 0.43	0.76 ± 0.58	0.99 ± 0.59	0.90 ± 0.81
300-450 ml	**inspiration**	24 (96%)	344 ± 33	-0.34 ± 0.90	-4.07 ± 1.09	4.37 ± 1.90	0.51 ± 0.56	0.73 ± 0.57	0.97 ± 0.69	1.33 ± 1.49
	expiration	25 (100%)	397 ± 19	2.58 ± 0.83	-6.85 ± 1.08	4.34 ± 1.39	0.74 ± 0.56	0.68 ± 0.60	1.07 ± 0.74	0.79 ± 0.59
>450 ml	**inspiration**	25 (100%)	469 ± 13	0.96 ± 1.21	-5.41 ± 0.74	4.50 ± 1.48	0.36 ± 0.45	0.49 ± 0.52	0.67 ± 0.63	3.67 ± 1.19
	expiration	25 (100%)	595 ± 21	3.10 ± 0.67	-8.93 ± 1.32	3.24 ± 1.94	0.65 ± 0.45	0.86 ± 0.55	1.17 ± 0.54	0.89 ± 0.56
respiratory bellows-based classification										
minimum - low	**inspiration**	25 (100%)	29 ± 26	0.26 ±1.01	-2.49 ± 0.64	5.05 ± 2.22	0.50± 0.42	0.63 ± 0.56	0.91 ± 0.56	1.19 ± 1.21
	expiration	25 (100%)	90 ± 70	2.08 ± 1.04	-4.11 ± 1.32	6.19 ± 1.64	0.47 ± 0.55	0.92 ± 0.73	1.14 ± 0.79	1.01 ± 0.65
low - medium	**inspiration**	25 (100%)	105 ± 59	-0.72 ± 1.11	-2.94 ± 0.60	6.15 ± 1.85	0.58 ± 0.45	0.67 ± 0.75	1.01 ± 0.74	1.09 ± 0.78
	expiration	25 (100%)	289 ± 67	2.78 ± 0.89	-6.06 ± 1.57	4.19 ± 1.67	0.36 ± 0.35	0.67 ± 0.61	0.84 ± 0.62	0.94 ± 0.70
medium - high	**inspiration**	25 (100%)	306 ± 58	-0.46 ± 1.03	-4.47 ± 0.79	5.19 ± 1.89	0.47 ± 0.40	0.78 ± 0.67	0.99 ± 0.69	0.88 ± 0.73
	expiration	25 (100%)	437 ± 32	2.06 ± 1.30	-7.20 ± 1.75	3.89 ± 1.79	0.72 ± 0.79	0.99 ± 0.96	1.34 ± 1.11	1.12 ± 0.99
high - maximum	**inspiration**	25 (100%)	496 ± 72	0.30 ± 1.73	-6.08 ± 1.45	3.67 ± 2.18	0.52 ± 0.57	0.81 ±0.67	1.03 ± 0.80	0.98 ± 1.07
	expiration	25 (100%)	490 ± 64	2.23 ± 1.16	-7.94 ± 2.10	4.17 ± 2.21	0.87 ± 0.84	1.10 ± 1.11	1.54 ± 1.25	1.54 ± 0.92
no respiratory classification										
no respiratory classification	**heart cycle #1**	25 (100%)	126 ± 145	0.55 ± 1.08	-2.80 ± 1.66	3.45 ± 2.07	0.92 ± 0.84	1.60 ± 1.29	1.91 ± 1.45	1.79 ± 1.65
	heart cycle #2	25 (100%)	579 ± 188	1.43 ± 1.86	-5.62 ± 1.91	2.78 ± 2.16	0.72 ± 0.85	1.35 ± 1.81	1.60 ± 1.94	1.23 ± 1.37
	heart cycle #3	25 (100%)	547 ± 97	2.61 ± 1.56	-6.50 ± 1.34	2.81 ± 2.10	1.10 ± 1.13	0.94 ± 1.18	1.68 ± 1.46	0.98 ± 1.25
	heart cycle #4	25 (100%)	280 ± 172	2.50 ± 1.05	-4.92 ± 1.70	3.25 ± 1.75	0.90 ± 0.79	1.73 ± 1.37	2.08 ± 1.41	1.15 ± 1.00
	heart cycle #5	25 (100%)	385 ± 191	1.13 ± 1.69	-4.96 ± 2.35	4.54 ± 1.95	1.06 ± 1.02	2.36 ± 1.81	2.72 ± 1.90	1.23 ± 0.84
	heart cycle #6	25 (100%)	381 ± 183	1.80 ± 1.58	-6.27 ± 2.12	3.92 ± 1.90	1.53 ± 1.06	2.29 ± 2.00	2.91 ± 2.07	1.08 ± 0.86
	heart cycle #7	25 (100%)	249 ± 237	1.85 ± 1.58	-5.54 ± 2.59	4.52 ± 2.22	1.00 ± 0.92	2.15 ± 1.88	2.47 ± 1.94	2.08 ± 1.20
	heart cycle #8	25 (100%)	251 ± 159	1.12 ± 1.41	-4.05 ± 2.18	5.41 ±2.25	1.50 ± 1.14	2.51 ± 2.37	3.08 ± 2.45	1.35 ± 1.04
mean of cycles classified by ECG and spirometry		**196 (98%)**	**269 ± 25**	**1.33 ± 1.01**	**-4.36 ± 0.93**	**4.84 ± 1.70**	**0.58 ± 0.55**	**0.65 ± 0.51**	**0.97 ± 0.65**	**1.32 ± 1.05**
mean of cycles classified by ECG and respiratory bellows		**200 (100%)**	**280 ± 56**	**1.07 ± 1.66**	**-5.16 ± 1.32**	**4.81 ± 1.93**	**0.56 ± 0.55**	**0.82 ± 0.76**	**1.10 ± 0.82**	**1.09 ± 0.88**
mean of cycles classified by ECG		**200 (100%)**	**350 ± 171**	**1.62 ± 1.48**	**-5.08 ± 1.98**	**3.84 ± 2.05**	**1.09 ± 0.97**	**1.87 ± 1.71**	**2.31 ± 1.83**	**1.36 ± 1.15**
p-value (ECG/spirometry vs. ECG)		**n.s.**	**n.s.**	**n.s.**	**n.s.**	**n.s.**	**<0.001**	**<0.001**	**<0.001**	**n.s.**
p-value (ECG/resp. bellows vs. ECG)		**n.s.**	**n.s.**	**n.s.**	**n.s.**	**n.s.**	**<0.001**	**<0.001**	**<0.001**	**<0.02**

Table 4. Motion control results of subject 1 (modified from Röwer LM et al. (38)).

respiratory volume	respiratory phase	number of phases (%)	mean spirometry volume (ml)	mean position (mm) and angulation (°)			mean displacement (mm) and rotation (°)			
				x-axis	y-axis	angulation	x-axis	y-axis	total	rotation
spirometry-based classification										
<200 ml	**inspiration**	25 (100%)	-6 ± 63	0.00 ± 1.39	0.00 ± 1.71	9.70 ± 1.92	0.70 ± 0.73	0.95 ± 1.14	1.29 ± 1.24	1.20 ± 1.33
	expiration	25 (100%)	-31 ± 9	2.16 ± 1.45	2.89 ± 1.06	8.41 ± 1.22	0.74 ± 0.80	0.63 ± 0.50	1.07 ± 0.83	0.73 ± 0.43
200-400 ml	**inspiration**	19 (76%)	268 ± 55	1.03 ± 0.55	-4.72 ± 1.62	6.56 ± 1.25	0.59 ± 0.42	0.64 ± 0.55	0.99 ± 0.50	1.19 ± 0.87
	expiration	25 (100%)	257 ± 53	5.29 ± 2.05	-2.95 ± 1.34	8.26 ± 1.55	0.83 ± 0.80	0.87 ± 0.93	1.30 ± 1.13	1.11 ± 0.84
400-600 ml	**inspiration**	21 (84%)	471 ± 54	3.76 ± 1.52	-7.86 ± 1.03	6.80 ± 1.79	0.72 ± 0.48	0.69 ± 0.63	1.10 ± 0.65	1.09 ± 0.70
	expiration	20 (80%)	458 ± 53	5.78 ± 1.83	-6.00 ± 1.10	6.84 ± 1.65	0.59 ± 0.51	1.03 ± 0.97	1.26 ± 0.94	1.56 ± 2.09
>600 ml	**inspiration**	25 (100%)	681 ± 60	2.84 ± 1.58	-11.95 ± 1.03	4.14 ± 1.65	0.76 ± 0.66	0.83 ± 0.71	1.23 ± 0.85	3.81 ± 1.84
	expiration	25 (100%)	708 ± 95	7.11 ± 1.70	-9.13 ± 1.52	4.67 ± 2.72	0.83 ± 0.81	0.94 ± 0.99	1.40 ± 1.12	1.22 ± 1.17
respiratory bellows-based classification										
minimum - low	**inspiration**	25 (100%)	-18 ± 10	-0.46 ± 0.95	0.59 ± 1.78	8.95 ± 0.98	0.38 ± 0.33	0.57 ± 0.76	0.82 ± 0.69	0.83 ± 0.74
	expiration	25 (100%)	36 ± 33	0.15 ± 1.22	-1.18 ± 1.65	9.12 ± 1.30	0.70 ± 1.01	1.01 ± 1.04	1.31 ± 1.07	0.90 ± 0.70
low - medium	**inspiration**	23 (92%)	436 ± 69	0.39 ± 1.15	-4.16 ± 1.82	7.41 ± 1.10	0.61 ± 0.45	0.86 ± 1.03	1.17 ± 1.00	1.14 ± 1.56
	expiration	25 (100%)	278 ± 66	2.13 ± 1.78	-6.84 ± 1.05	6.71 ± 2.40	0.92 ± 0.77	0.70 ± 0.82	1.29 ± 0.97	1.64 ± 1.67
medium - high	**inspiration**	23 (92%)	716 ± 64	0.85 ± 0.84	-8.78 ± 1.18	6.48 ± 2.34	0.64 ± 0.42	0.94 ± 0.96	1.22 ± 0.94	1.03 ± 1.07
	expiration	25 (100%)	458 ± 45	3.47 ± 1.44	-10.55 ± 1.75	2.81 ±2.17	0.69 ± 0.65	0.66 ± 0.69	1.11 ± 0.75	1.27 ± 1.17
high - maximum	**inspiration**	24 (96%)	889 ± 25	2.27 ± 0.78	-12.57 ± 1.01	4.41 ± 1.40	0.63 ± 0.62	0.87 ± 0.90	1.12 ± 1.04	0.83 ± 0.72
	expiration	25 (100%)	814 ± 93	3.34 ± 1.28	-13.66 +/ 1.14	2.08 ± 1.48	0.56 ± 0.68	0.66 ± 0.64	0.99 ± 0.80	0.80 ± 0.94
no respiratory classification										
no respiratory classification	**heart cycle #1**	25 (100%)	769 ± 337	6.54 ± 2.00	-10.51 ± 4.65	3.97 ± 2.89	1.89 ± 1.92	4.34 ± 5.09	4.89 ± 5.30	3.22 ± 3.18
	heart cycle #2	25 (100%)	415 ± 178	5.76 ± 1.94	-6.03 ± 2.78	7.00 ± 1.95	1.09 ± 0.97	1.91 ± 1.80	2.37 ± 1.84	1.50 ± 1.41
	heart cycle #3	25 (100%)	161 ± 283	2.26 ± 2.16	-1.93 ± 5.21	8.45 ± 2.78	2.01 ± 2.18	4.55 ± 5.82	5.33 ± 6.29	2.79 ± 2.51
	heart cycle #4	25 (100%)	211 ± 321	1.50 ± 2.33	-3.47 ± 6.07	6.40 ± 2.48	2.43 ± 2.06	7.15 ± 6.48	7.65 ± 6.69	3.12 ± 2.25
	heart cycle #5	25 (100%)	577 ± 233	5.72 ± 1.65	-7.74 ± 3.91	5.27 ± 2.25	1.53 ± 1.21	3.09 ± 3.00	3.77 ± 2.86	1.46 ± 1.30
	heart cycle #6	25 (100%)	635 ± 399	5.74 ± 2.71	-8.77 ± 6.27	5.15 ± 2.63	2.61 ± 1.97	7.77 ± 5.17	8.30 ± 5.37	2.27 ± 2.09
	heart cycle #7	25 (100%)	501 ± 408	4.47 ± 2.16	-8.77 ± 6.02	6.57 ± 2.69	3.05 ± 1.95	6.89 ± 5.39	7.70 ± 5.23	3.33 ± 2.61
	heart cycle #8	25 (100%)	385 ± 379	4.35 ± 2.33	-5.54 ± 5.56	7.48 ± 2.13	2.14 ± 1.60	4.69 ± 3.71	5.34 ± 3.79	2.51 ± 1.65
mean of cycles classified by ECG and spirometry		**185 (92.5%)**	**351 ± 55**	**3.50 ± 1.51**	**-4.96 ± 1.30**	**6.92 ± 1.72**	**0.72 ± 0.65**	**0.82 ± 0.80**	**1.21 ± 0.91**	**1.48 ± 1.16**
mean of cycles classified by ECG and respiratory bellows		**195 (97.5%)**	**451 ± 42**	**1.52 ± 0.94**	**-7.14 ± 1.42**	**6.00 ± 1.62**	**0.64 ± 0.62**	**0.78 ± 0.86**	**1.13 ± 0.91**	**1.06 ± 1.07**
mean of cycles classified by ECG		**200 (100%)**	**457 ± 317**	**4.54 ± 2.16**	**-6.59 ± 5.06**	**6.28 ± 2.48**	**2.09 ± 1.73**	**5.05 ± 4.56**	**5.67 ± 4.67**	**2.53 ± 2.12**
p-value (ECG/spirometry vs. ECG)		**n.s.**	**n.s.**	**n.s.**	**n.s.**	**n.s.**	**<0.001**	**<0.001**	**<0.001**	**<0.001**
p-value (ECG/resp. bellows vs. ECG)		**n.s.**	**n.s.**	**n.s.**	**n.s.**	**n.s.**	**<0.001**	**<0.001**	**<0.001**	**<0.001**

Table 5. Motion control results of subject 2 (modified from Röwer LM et al. (38)).

respiratory volume	respiratory phase	number of phases (%)	mean spirometry volume (ml)	mean position (mm) and angulation (°)			mean displacement (mm) and rotation (°)			
				x-axis	y-axis	angulation	x-axis	y-axis	total	rotation
spirometry-based classification										
<200 ml	**inspiration**	25 (100%)	-3 ± 28	0.00 ± 0.98	0.00 ± 1.33	-2.60 ± 1.97	0.60 ± 0.62	1.12 ± 1.08	1.37 ± 1.14	1.08 ± 0.98
	expiration	25 (100%)	-3 ± 10	0.96 ± 0.70	1.15 ± 0.95	-1.46 ± 1.75	0.53 ± 0.45	0.58 ± 0.63	0.89 ± 0.65	0.86 ± 0.60
200-400 ml	**inspiration**	20 (80%)	265 ± 58	2.19 ± 1.73	-4.08 ± 1.21	-4.74 ± 2.61	0.76 ± 0.80	0.83 ± 0.72	1.28 ± 0.90	1.18 ± 1.21
	expiration	25 (100%)	263 ± 48	2.90 ± 0.92	0.74 ± 1.04	-2.03 ± 2.14	0.66 ± 0.53	0.86 ± 0.91	1.20 ± 0.91	1.15 ± 0.86
400-600 ml	**inspiration**	23 (96%)	480 ± 59	3.45 ± 1.20	-4.55 ± 0.96	-6.45 ± 3.22	0.57 ± 0.56	0.73 ± 0.76	1.08 ± 0.77	1.39 ± 1.38
	expiration	24 (96%)	474 ± 54	4.03 ± 1.02	-0.65 ± 0.68	-3.10 ± 2.03	0.48 ± 0.41	0.70 ± 0.53	0.91 ±0.55	1.08 ± 0.86
>600 ml	**inspiration**	25 (100%)	673 ± 49	4.92 ± 1.41	-5.14 ± 0.98	-7.17 ± 2.76	0.74 ± 0.64	0.84 ± 0.60	1.21 ± 0.73	1.24 ± 1.16
	expiration	24 (96%)	694 ± 91	4.53 ± 0.91	-1.33 ± 1.26	-4.03 ± 3.07	0.45 ± 0.39	1.04 ± 1.19	1.19 ± 0.84	1.20 ± 0.96
respiratory bellows-based classification										
minimum - low	**inspiration**	25 (100%)	194 ± 94	2.80 ± 1.00	0.65 ± 0.71	-2.44 ± 1.82	0.91 ± 0.79	0.57 ±0.47	1.15 ± 0.82	0.66 ± 0.60
	expiration	22 (92%)	350 ± 79	3.87 ± 0.62	0.27 ± 1.29	-2,57 ± 2.24	0.51 +/. 0.47	1.19 ± 1.03	1.38 ± 1.03	0.94 ± 0.84
low - medium	**inspiration**	23 (92%)	52 ± 74	1.75 ± 0.70	1.27 ± 0.55	-1.67 ± 2.14	0.42 ± 0.42	0.45 ± 0.46	0.66 +/ 0.58	0.71 ± 0.75
	expiration	22 (88%)	502 ± 203	4.35 ± 1.15	0.27 ± 1.30	-3.32 ± 2.22	0.55 ± 0.44	0.98 ± 0.99	1.20 ± 0.99	1.03 ± 0.87
medium - high	**inspiration**	25 (100%)	263 ± 149	2.87 ± 1.67	-3.38 ± 0.71	-5.71 ± 2.77	0.74 ± 0.61	0.71 ± 0.57	1.18 ± 0.60	1.17 ± 0.89
	expiration	25 (100%)	974 ± 58	6.60 ± 1.24	-3.74 ± 0.89	-6.60 ± 2.55	0.57 ± 0.32	0.55 ± 0.48	0.85 ± 0.48	0.97 ± 0.80
high - maximum	**inspiration**	25 (100%)	620 ± 111	4.29 ± 1.63	-4.37 /- 1.18	-7.21 ± 2.72	1.05 ± 1.12	0.76 ± 0.67	1.46 ± 1.11	1.29 ± 1.16
	expiration	25 (100%)	911 ± 57	7.01 ± 1.37	-4.72 ± 1.14	-7.14 ± 2.75	0.51 ± 0.42	0.97 ± 0.83	1.24 ± 0.74	1.06 ± 1.12
no respiratory classification										
no respiratory classification	**heart cycle #1**	25 (100%)	171 ± 341	0.44 ± 1.93	-2.33 ± 2.88	-2.50 ± 3.46	2.30 ± 2.12	3.19 ± 2.59	4.03 ± 3.23	3.28 ± 2.37
	heart cycle #2	25 (100%)	362 ± 278	2.25 ± 1.89	-5.08 ± 2.12	-6.45 ± 2.08	2.00 ± 1.31	1.73 ± 1.73	2.91 ± 1.81	1.34 ± 1.01
	heart cycle #3	25 (100%)	737 ± 291	4.59 ± 2.41	-6.46 ± 2.88	-7.02 ± 3.42	1.91 ± 1.70	2.45 ± 1.88	3.55 ± 1.87	2.91 ± 2.71
	heart cycle #4	25 (100%)	828 ± 354	4.58 ± 2.59	-5.02 ± 2.87	-6.05 ± 3.04	2.21 ± 1.82	2.63 ± 2.67	3.60 ± 3.05	3.20 ± 2.37
	heart cycle #5	25 (100%)	618 ± 287	2.98 ± 1.69	-2.32 ± 1.84	-5.39 ± 3.13	1.47 ± 1.20	1.76 ± 1.67	2.46 ± 1.85	2.57 ± 2.27
	heart cycle #6	25 (100%)	326 ± 233	1.99 ± 1.51	-1.08 ± 2.45	-3.86 ± 2.92	1.22 ± 1.35	2.19 ± 2.53	2.74 ± 2.64	2.40 ± 2.37
	heart cycle #7	25 (100%)	145 ± 268	1.02 ± 1.62	-1.48 ± 2.88	-3.49 ± 2.33	1.37 ± 1.26	2.68 ± 2.66	3.25 ± 2.67	2.22 ± 2.00
	heart cycle #8	25 (100%)	214 ± 264	1.42 ± 1.65	-3.03 ± 2.24	-5.06 ± 3.85	1.71 ± 1.46	1.94 ± 1.86	2.85 ± 2.04	2.31 ± 2.04
mean of cycles classified by ECG and spirometry		**191 (96%)**	**355 ± 50**	**2.87 ± 1.11**	**-1.73 ± 1.05**	**-3.95 ± 2.44**	**0.60 ± 0.55**	**0.84 ± 0.76**	**1.14 ± 0.17**	**1.15 ± 1.00**
mean of cycles classified by ECG and respiratory bellows		**192 (96%)**	**483 ± 103**	**4.19 ± 1.17**	**-1.80 ± 0.97**	**-4.58 ± 2.40**	**0.66 ± 0.57**	**0.77 ± 0.69**	**1.14 ± 0.79**	**0.98 ± 0.88**
mean of cycles classified by ECG		**200 (100%)**	**425 ± 290**	**2.41 ± 1.91**	**-3.35 ± 2.52**	**-4.98 ± 3.03**	**1.77 ± 1.53**	**2.32 ± 2.20**	**3.17 ± 0.54**	**2.53 ± 2.14**
p-value (ECG/spirometry vs. ECG)		**n.s.**	**n.s.**	**n.s.**	**n.s.**	**n.s.**	**<0.001**	**<0.001**	**<0.001**	**<0.001**
p-value (ECG/resp. bellows vs. ECG)		**n.s.**	**n.s.**	**n.s.**	**n.s.**	**n.s.**	**<0.001**	**<0.001**	**<0.001**	**<0.001**

Table 6. Motion control results of subject 3 (modified from Röwer LM et al. (38)).

respiratory volume	respiratory phase	number of phases (%)	mean spirometry volume (ml)	mean position (mm) and angulation (°)			mean displacement (mm) and rotation (°)			
				x-axis	y-axis	angulation	x-axis	y-axis	total	rotation
spirometry-based classification										
<70 ml	inspiration	25 (100%)	11 ± 23	0.00 ± 1.05	0.00 ± 1.17	-8.20 ± 4.84	0.48 ± 0.47	0.75 ± 0.75	0.99 ± 0.76	1.85 ± 1.44
	expiration	25 (100%)	6 ± 19	0.45 ± 1.11	-0.97 ± 1.32	-7.11 ± 4.20	0.62 ± 0.53	0.86 ± 0.62	1.13 ± 0.71	1.50 ± 1.05
70-140 ml	inspiration	25 (100%)	83 ± 14	-0.59 ± 0.87	-1.67 ± 1.25	-9.12 ± 3.90	0.52 ± 0.29	0.74 ± 0.71	1.01 ± 0.64	1.54 ± 1.77
	expiration	24 (96%)	90 ± 16	2.33 ± 0.87	-2.32 ± 1.42	-7.90 ± 4.04	0.42 ± 0.37	0.62 ± 0.65	0.84 ± 0.63	1.41 ± 1.18
140-210 ml	inspiration	25 (100%)	164 ± 21	0.11 ± 0.92	-2.39 ± 0.91	-11.25 ± 4.26	0.67 ± 0.56	0.73 ± 0.58	1.07 ± 0.67	1.87 ± 1.98
	expiration	24 (96%)	165 ± 20	2.67 ± 0.75	-3.69 ± 0.88	-8.00 ± 3.90	0.50 ± 0.32	0.70 ± 0.58	0.94 ± 0.57	1.16 ± 1.01
>210 ml	inspiration	25 (100%)	232 ± 16	0.57 ± 0.56	-4.97 ± 1.32	-11.19 ± 3.77	0.38 ± 0.29	0.90 ± 0.76	1.05 ± 0.72	1.60 ± 1.27
	expiration	25 (100%)	235 ± 21	2.43 ± 0.59	-4.55 ± 1.05	-8.92 ± 3.60	0.51 ± 0.46	0.87 ± 0.67	1.10 ± 0.70	1.54 ± 1.23
no respiratory classification										
no respiratory classification	heart cycle #1	25 (100%)	96 ± 116	-16.54 ± 1.01	2.34 ± 3.10	-6.37 ± 4.67	0.96 ± 0.68	2.50 ± 2.74	2.85 ± 2.65	2.67 ± 2.33
	heart cycle #2	25 (100%)	131 ± 108	-16.91 ± 1.74	2.00 ± 3.11	-7.36 ± 4.17	1.36 ± 1.10	2.39 ± 2.08	2.92 ± 2.14	2.18 ± 1.40
	heart cycle #3	25 (100%)	242 ± 60	-16.23 ± 1.53	-0.02 ± 1.95	-8.03 ± 3.99	0.90 ± 0.88	1.73 ± 1.74	2.14 ± 1.26	1.99 ± 1.46
	heart cycle #4	25 (100%)	234 ± 89	-16.43 ± 1.56	0.31 ± 2.61	-8.16 ± 3.94	0.77 ± 0.62	2.27 ± 2.06	2.56 ± 1.96	2.11 ± 1.41
	heart cycle #5	25 (100%)	215 ± 91	-16.45 ± 0.96	-0.09 ± 3.14	-7.86 ± 4.00	0.84 ± 0.75	2.83 ± 1.84	3.07 ± 1.80	2.10 ± 1.42
	heart cycle #6	25 (100%)	210 ± 103	-16.10 ± 1.13	0.15 ± 3.08	-6.90 ± 4.20	1.00 ± 0.64	3.25 ± 2.59	3.53 ± 2.50	2.19 ± 1.65
	heart cycle #7	25 (100%)	176 ± 120	-16.43 ± 1.53	0.15 ± 2.88	-7.72 ± 4.87	1.02 ± 0.84	2.63 ± 2.18	2.99 ± 2.11	2.08 ± 2.56
	heart cycle #8	25 (100%)	231 ± 86	-16,57 ± 1.56	0.88 ± 3.07	-6.92 ± 3.24	1.14 ± 0.91	3.35 ± 2.13	3.71 ± 2.04	2.12 ± 1.16
mean of cycles classified by ECG and spirometry		**198 (99%)**	**123 ± 19**	**1.00 ± 0.84**	**-2.57 ± 1.16**	**-8.96 ± 4.06**	**0.51 ± 0.41**	**0.77 ± 0.66**	**1.02 ± 0.68**	**1.56 ± 1.37**
mean of cycles classified by ECG		**200 (100%)**	**191 ± 97**	**-16.46 ± 1.38**	**0.71 ± 2.87**	**-7.42 ± 4.14**	**1.00 ± 0.80**	**2.62 ± 2.17**	**2.97 ± 2.06**	**2.18 ± 1.67**
p-value (ECG/spirometry vs. ECG)		**n.s.**	**n.s.**	**n.s.**	**n.s.**	**n.s.**	**<0.001**	**<0.001**	**<0.001**	**<0.001**

Table 7. Motion control results of subject 4 (modified from Röwer LM et al. (38)).

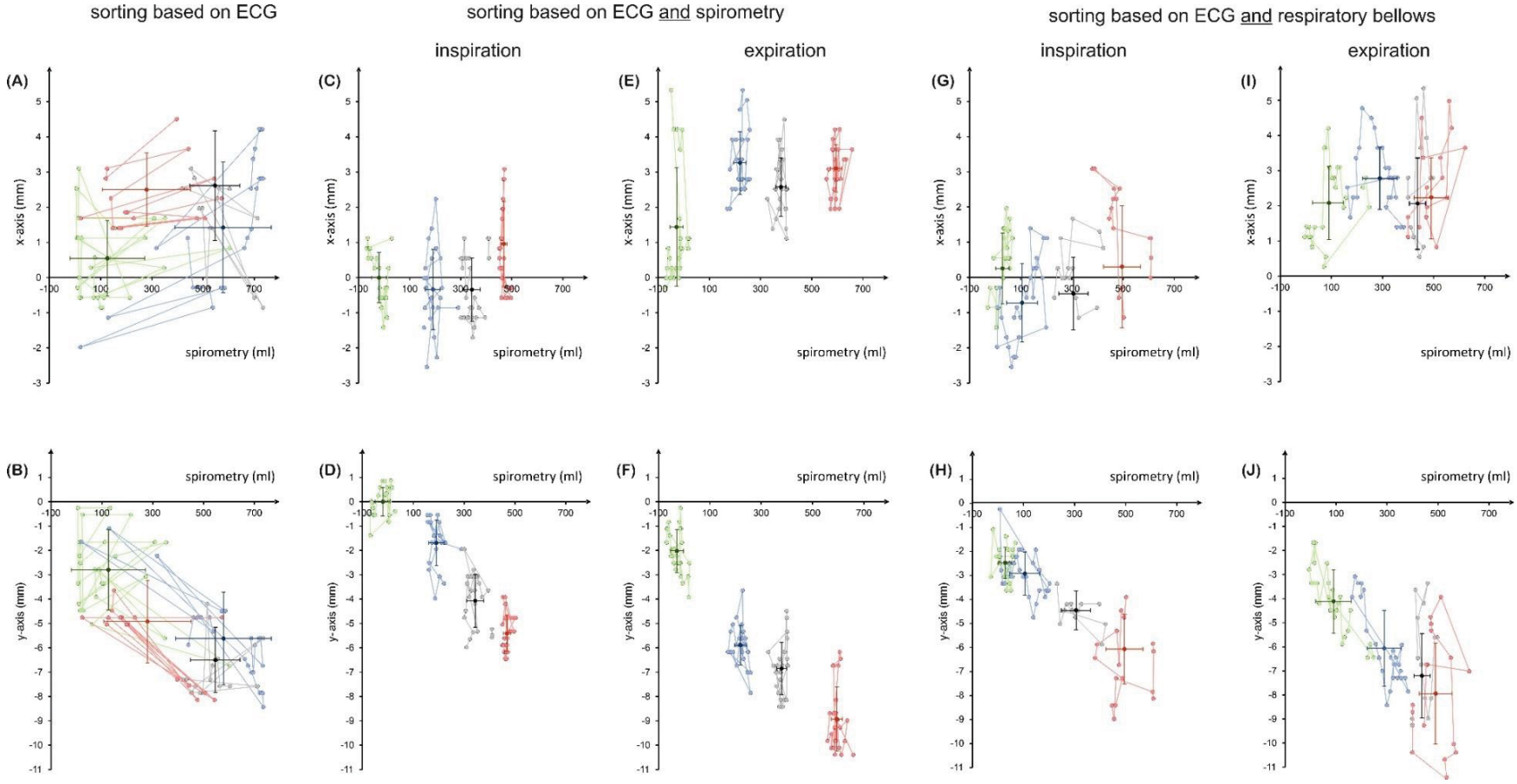

Figure 23. Motion control.

Cardiac cycles solely binned with ECG information resulted in strongly moving sequences with a pronounced motion in the direction of the x-axis (A) and y-axis (B). In contrast, the motion in heart cycles binned with ECG and respiratory information both with spirometry (C-F) and respiratory bellows (G-J) achieved a significant movement reduction for the direction in the x- and y-axis (modified from Röwer LM et al. (38)).

3.5 Left ventricular eccentricity index

The left ventricular end-diastolic eccentricity index (EId) was significantly modified by lung volume in the context of heart-lung interactions, whereas there was no influence on the end-systolic left ventricular eccentricity index (EIs) during free-breathing **(Figure 24A-D), (Tables 2-9)**.

The mean EId increased during inspiration from the respiratory class minimum-low to high-maximum from 1.17 ± 0.10 to 1.31 ± 0.13 (endocardial contouring) and from 1.04 ± 0.04 to 1.19 ± 0.05 (epicardial contouring) **(Figure 24A).**

Similar results were achieved during expiration **(Figure 24C).**

Linear regression of the increasing of the EId with increasing lung volume during inspiration and expiration demonstrates statistical significance (EId inspiration epicardial: R^2=0.95, $p<0.05$; EId expiration epicardial: R^2=0.97, $p<0.05$; EId inspiration endocardial: R^2=0.97, $p<0.05$; EId expiration endocardial: R^2=0.92, $p<0.05$).

Epicardial and endocardial LV eccentricity contouring achieved similar results. However, the epicardial contour could be more easily delineated, resulting in a lower standard deviation.

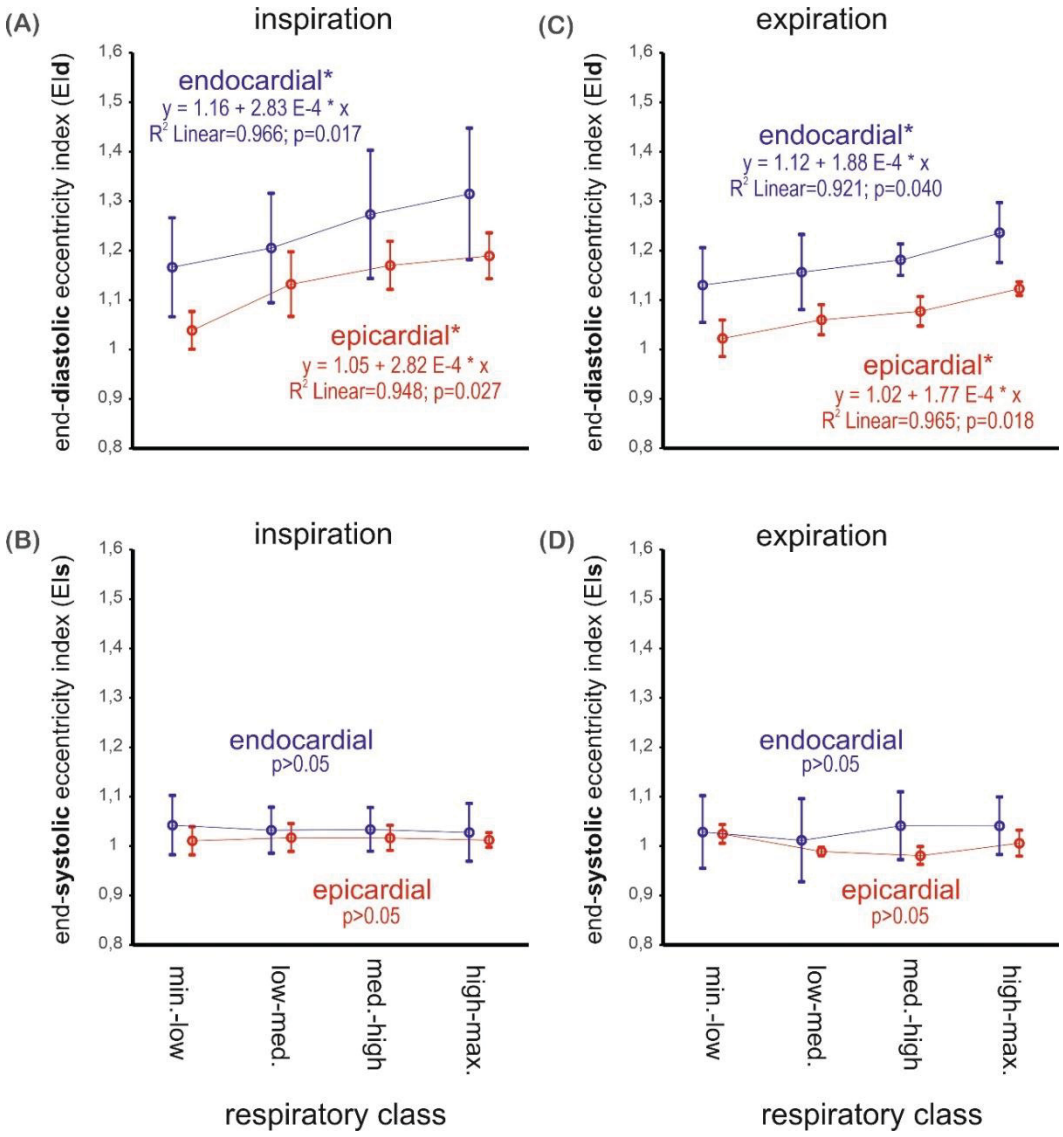

Figure 24. Left ventricular eccentricity index.

Mean results from the analysis of left ventricular eccentricity index for epicardial and endocardial contouring at end-diastole (EId) and end-systole (EIs) as a function of the spirometry volume and respiratory phase of four subjects. Circles represent the mean values, whiskers standard deviation. Linear regression results are presented in the corresponding graphs. Significant results with $p<0.05$ are marked with *. The unit of the x-axis is lung volume in ml. The EId increased in inspiration and expiration with higher lung volume both for epicardial and endocardial contouring (A, C). In contrast, the EIs was not influenced by respiration (B, D) (modified from Röwer LM et al. (38)).

heart phase	respiratory class		spirometry volume (ml)	epicardial contouring left ventricle		
	lung volume (ml)	respiratory phase		horizontal diameter (mm)	vertical diameter (mm)	eccentricity index
end-diastolic	<150	inspiration	29.87	75.47	76.26	1.0105
		expiration	-68.64	75.52	75.52	1.000
	150-300	inspiration	190.90	70.90	77.26	1.0897
		expiration	157.70	74.22	77.70	1.0375
	300-450	inspiration	408.56	67.03	78.29	1.1680
		expiration	357.76	72.65	77.90	1.0723
	>450	inspiration	450.82	67.19	78.94	1.1749
		expiration	573.19	69.77	77.77	1.1147
end-systolic	<150	inspiration	-30.15	67.26	64.88	0.9646
		expiration	-40.31	66.02	67.26	1.0188
	150-300	inspiration	226.93	66.14	65.24	0.9864
		expiration	209.42	65.81	65.70	0.9983
	300-450	inspiration	321.03	65.43	64.70	0.9888
		expiration	399.41	66.43	64.40	0.9694
	>450	inspiration	468.93	65.35	64.50	0.9870
		expiration	466.41	66.40	64.40	0.9699

Table 8. LV-EI: Epicardial contouring subject 1.

heart phase	respiratory class		spirometry volume (ml)	endocardial contouring left ventricle		
	lung volume (ml)	respiratory phase		horizontal diameter (mm)	vertical diameter (mm)	eccentricity index
end-diastolic	<150	inspiration	29.87	58.00	58.15	1.0026
		expiration	-68.64	58.10	58.61	1.0088
	150-300	inspiration	190.90	57.16	58.31	1.0201
		expiration	157.70	56.96	58.45	1.0262
	300-450	inspiration	408.56	52.66	55.48	1.0536
		expiration	357.76	51.39	58.54	1.1391
	>450	inspiration	450.82	51.95	56.72	1.0918
		expiration	573.19	50.56	57.74	1.1420
end-systolic	<150	inspiration	-30.15	37.68	36.04	0.9565
		expiration	-40.31	39.62	38.01	0.9594
	150-300	inspiration	226.93	37.51	37.22	0.9923
		expiration	209.42	37.68	36.85	0.9780
	300-450	inspiration	321.03	37.65	36.88	0.9795
		expiration	399.41	36.80	37.61	1.0220
	>450	inspiration	468.93	37.70	37.50	0.9947
		expiration	466.41	38.82	38.81	0.9997

Table 9. LV-EI: Endocardial contouring subject 1.

heart phase	respiratory class		spirometry volume (ml)	epicardial contouring left ventricle		
	lung volume (ml)	respiratory phase		horizontal diameter (mm)	vertical diameter (mm)	eccentricity index
end-diastolic	<200	inspiration	7.32	78.42	79.26	1.0107
		expiration	-46.27	78.66	80.20	1.0196
	200-400	inspiration	343.45	76.44	82.43	1.0784
		expiration	231.20	77.20	82.40	1.0674
	400-600	inspiration	401.34	76.02	84.42	1.1105
		expiration	554.17	76.00	84.80	1.1158
	>600	inspiration	674.24	75.20	84.82	1.1279
		expiration	644.60	75.63	84.42	1.1162
end-systolic	<200	inspiration	-23.85	72.43	73.27	1.0116
		expiration	-64.98	72.40	73.60	1.0166
	200-400	inspiration	312.85	71.69	71.64	0.9993
		expiration	361.48	72.85	71.71	0.9844
	400-600	inspiration	548.67	71.29	72.05	1.0107
		expiration	459.97	73.31	73.76	1.0061
	>600	inspiration	602.56	70.49	71.63	1.0162
		expiration	600.92	70.16	72.62	1.0351

Table 10. LV-EI: Epicardial contouring subject 2.

heart phase	respiratory class		spirometry volume (ml)	endocardial contouring left ventricle		
	lung volume (ml)	respiratory phase		horizontal diameter (mm)	vertical diameter (mm)	eccentricity index
end-diastolic	<200	inspiration	7.32	53.60	62.83	1.1722
		expiration	-46.27	52.84	62.73	1.1872
	200-400	inspiration	343.45	52.45	64.04	1.2210
		expiration	231.20	53.61	64.80	1.2087
	400-600	inspiration	401.34	49.21	68.02	1.3822
		expiration	554.17	53.61	65.20	1.2162
	>600	inspiration	674.24	48.46	68.66	1.4168
		expiration	644.60	52.41	65.24	1.2448
end-systolic	<200	inspiration	-23.85	39.23	40.42	1.0303
		expiration	-64.98	41.08	40.78	0.9927
	200-400	inspiration	312.85	39.33	39.40	1.0018
		expiration	361.48	41.21	39.61	0.9612
	400-600	inspiration	548.67	40.07	40.53	1.0115
		expiration	459.97	41.32	41.04	0.9932
	>600	inspiration	602.56	41.76	41.79	1.0007
		expiration	600.92	41.30	41.92	1.0150

Table 11. LV-EI: Endocardial contouring subject 2.

heart phase	respiratory class		spirometry volume (ml)	epicardial contouring left ventricle		
	lung volume (ml)	respiratory phase		horizontal diameter (mm)	vertical diameter (mm)	eccentricity index
end-diastolic	<150	inspiration	5.74	73.93	81.56	1.1032
		expiration	-11.07	75.20	81.44	1.0830
	150-300	inspiration	232.60	66.59	82.73	1.2424
		expiration	207.62	74.84	82.81	1.1065
	300-450	inspiration	515.82	66.94	83.39	1.2457
		expiration	empty	empty	empty	empty
	>450	inspiration	751.37	66.88	84.06	1.2569
		expiration	956.10	73.60	84.40	1.1467
end-systolic	<150	inspiration	-22.46	67.34	70.13	1.0414
		expiration	17.91	66.82	70.59	1.0564
	150-300	inspiration	244.13	64.12	68.03	1.0610
		expiration	278.88	68.57	68.26	0.9955
	300-450	inspiration	495.93	64.53	64.79	1.0040
		expiration	536.64	65.93	68.13	1.0334
	>450	inspiration	681.78	63.00	64.24	1.0197
		expiration	647.85	68.73	70.53	1.0262

Table 12. LV-EI: Epicardial contouring subject 3.

heart phase	respiratory class		spirometry volume (ml)	endocardial contouring left ventricle		
	lung volume (ml)	respiratory phase		horizontal diameter (mm)	vertical diameter (mm)	eccentricity index
end-diastolic	<150	inspiration	5.74	56.47	69.20	1.2254
		expiration	-11.07	57.48	68.96	1.1997
	150-300	inspiration	232.60	53.44	68.53	1.2824
		expiration	207.62	57.67	69.92	1.2105
	300-450	inspiration	515.82	52.56	68.67	1.3065
		expiration	empty	empty	empty	empty
	>450	inspiration	751.37	51.29	68.46	1.3348
		expiration	956.10	56.41	70.32	1.2466
end-systolic	<150	inspiration	-22.46	39.73	44.64	1.1236
		expiration	17.91	42.67	49.15	1.1519
	150-300	inspiration	244.13	38.21	42.42	1.1102
		expiration	278.88	40.49	46.82	1.1563
	300-450	inspiration	495.93	38.83	40.57	1.0448
		expiration	536.64	39.39	45.85	1.1640
	>450	inspiration	681.78	40.96	40.41	0.9866
		expiration	647.85	41.05	46.86	1.1415

Table 13. LV-EI: Endocardial contouring subject 3.

heart phase	respiratory class		spirometry volume (ml)	epicardial contouring left ventricle		
	lung volume (ml)	respiratory phase		horizontal diameter (mm)	vertical diameter (mm)	eccentricity index
end-diastolic	<70	inspiration	47.20	53.60	55.21	1.0300
		expiration	8.71	56.81	56.04	0.9864
	70-140	inspiration	77.84	50.81	56.82	1.1183
		expiration	136.97	56.02	57.62	1.0286
	140-210	inspiration	158.47	48.80	56.40	1.1557
		expiration	159.50	55.80	58.20	1.0430
	>210	inspiration	231.15	48.46	58.05	1.1979
		expiration	294.37	52.80	58.80	1.1136
end-systolic	<70	inspiration	-1.12	50.06	51.31	1.0250
		expiration	-10.04	48.77	49.08	1.0064
	70-140	inspiration	107.03	50.37	51.49	1.0222
		expiration	88.52	51.56	50.41	0.9777
	140-210	inspiration	142.13	48.66	51.10	1.0501
		expiration	149.92	50.97	49.27	0.9666
	>210	inspiration	213.83	48.87	50.13	1.0258
		expiration	215.14	50.86	50.46	0.9921

Table 14. LV-EI: Epicardial contouring subject 4.

heart phase	respiratory class		spirometry volume (ml)	endocardial contouring left ventricle		
	lung volume (ml)	respiratory phase		horizontal diameter (mm)	vertical diameter (mm)	eccentricity index
end-diastolic	<70	inspiration	47.20	40.80	51.60	1.2647
		expiration	8.71	44.81	50.41	1.1250
	70-140	inspiration	77.84	40.40	52.41	1.2973
		expiration	136.97	44.42	52.40	1.1796
	140-210	inspiration	158.47	38.80	52.40	1.3505
		expiration	159.50	45.10	53.61	1.1887
	>210	inspiration	231.15	36.85	52.15	1.4152
		expiration	294.37	42.40	55.60	1.3113
end-systolic	<70	inspiration	-1.12	28.63	30.32	1.0590
		expiration	-10.04	29.08	29.37	1.0100
	70-140	inspiration	107.03	28.80	29.50	1.0243
		expiration	88.52	31.76	30.22	0.9515
	140-210	inspiration	142.13	28.16	30.95	1.0991
		expiration	149.92	30.61	30.78	1.0056
	>210	inspiration	213.83	26.91	30.37	1.1286
		expiration	215.14	30.22	30.45	1.0076

Table 15. LV-EI: Endocardial contouring subject 4.

3.6 Respiratory influence on ventricular shape and volumetry

The respiratory influence on the left and right ventricle was already apparent when images from defined phases of the cardiac cycle but different respiratory classes were considered. Therefore, images from the same midventricular slice and from the same ECG classes (e.g., end-diastole and end-systole) were arranged for visual evaluation **(Figures 25, 26)**, **(Video link to the supplemental digital content:** https://onlinelibrary.wiley.com/action/downloadSupplement?doi=10.1002%2Fmrm.28892_&file=mrm28892-sup-0003-VideoS3.mp4 **)**.

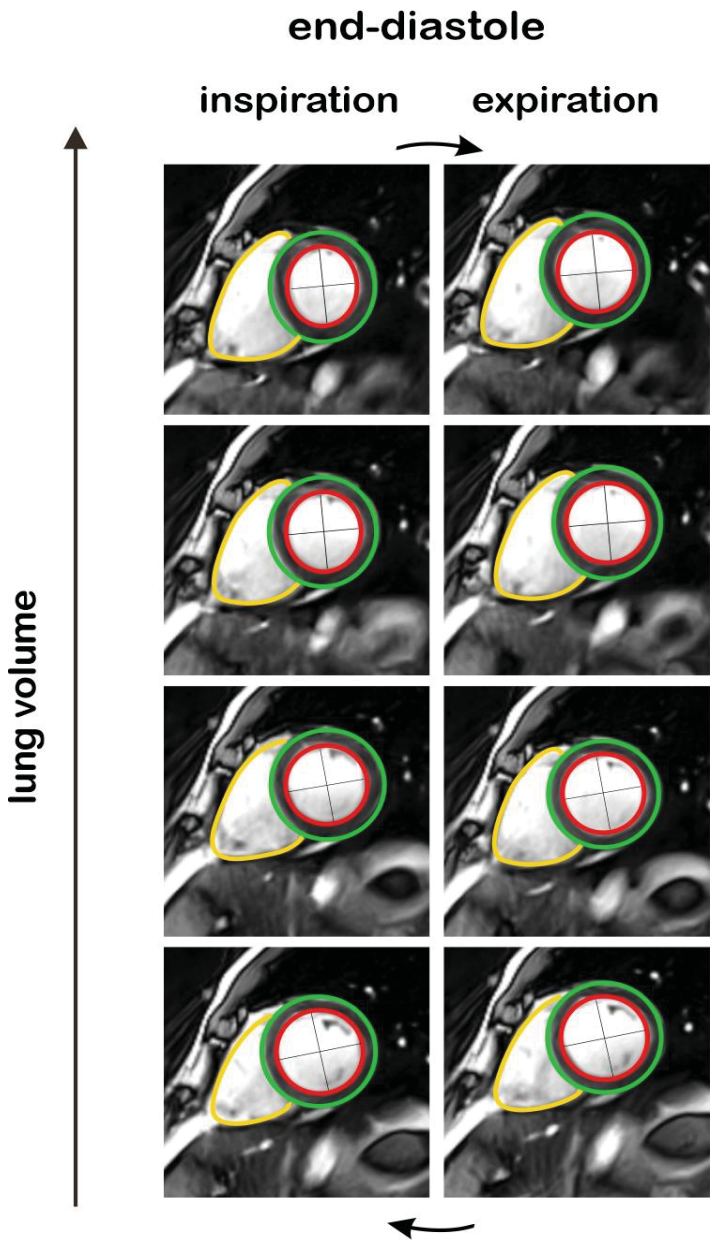

Figure 25. Visual assessment of left and right ventricle during end-diastole. During inspiration, the right ventricle becomes rounded, while the left ventricle turns from a circle to an ellipse with increasing lung volume.

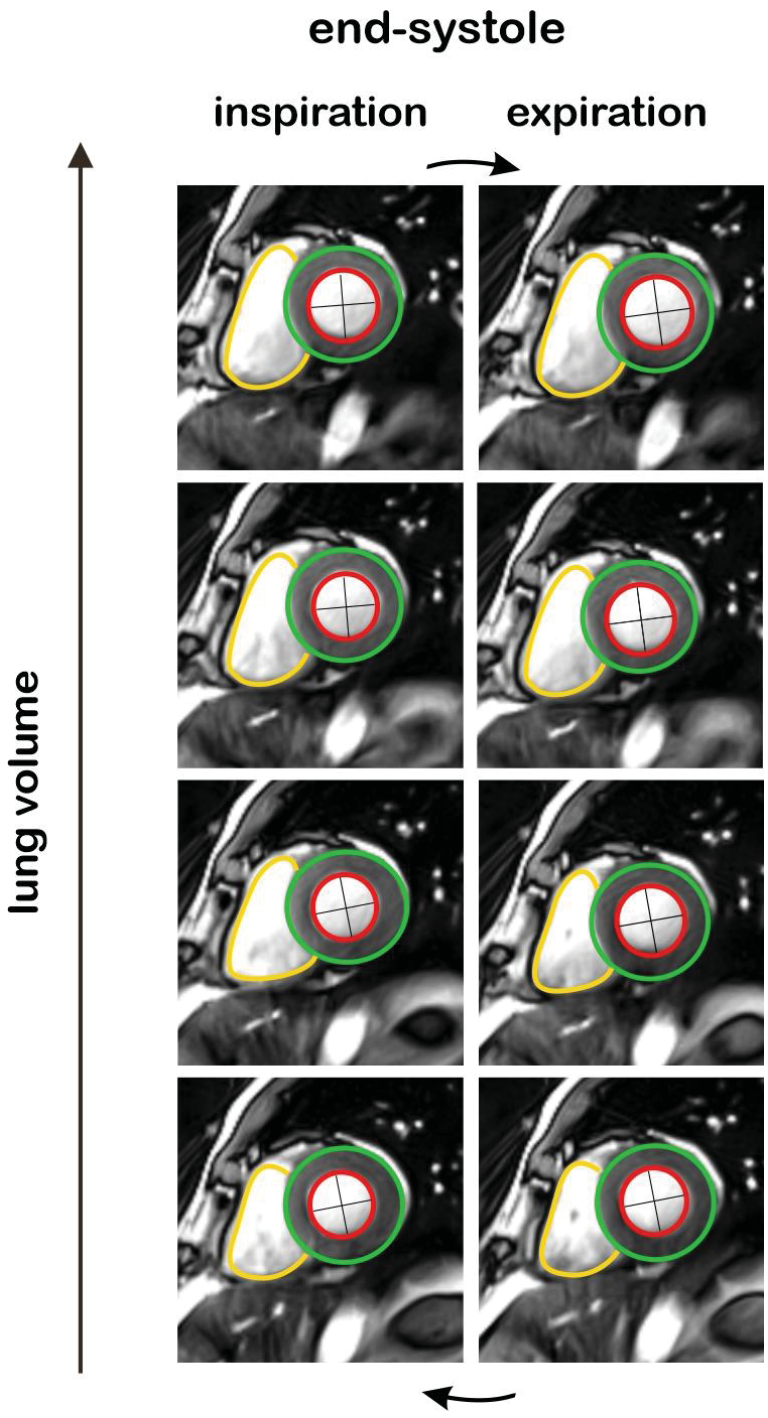

Figure 26. Visual assessment of left and right ventricle during end-systole. The left and right ventricular shape is not influenced by respiration during end-systole.

3.6.1 Right ventricle

A comparison of the right ventricle at different defined time points during the cardiac cycle in the different respiratory classes already showed clear differences of the ventricular shape. Especially during inspiration, the ventricle becomes rounded and loses its triangular configuration resulting from a higher preload. During expiration, it then resumes its original triangular shape. This effect is especially pronounced during end-diastole, whereas in end-systole there are hardly any differences in visual assessment **(Figures 25, 26)**.

The evaluation of the right ventricular volumetry confirmed the results of visual analysis. The largest effect of respiration on right ventricular volume was achieved for the right ventricular end-diastolic volume (RV-EDVi), stroke volume (RV-SVi) and for the right ventricular ejection fraction (RV-EF). These parameters showed a significant increase with increasing lung volume during inspiration for all subjects. In contrast, the end-systolic volume remained nearly unchanged. The largest effect was observed for the right ventricular end-diastolic volume from the lowest to the highest spirometry class during inspiration (79 ± 17 ml/m² to 98 ± 18 ml/m²). This was paralleled by an increase of the right ventricular stroke volume (41 ± 8 ml/m² to 59 ± 11 ml/m²) **(Figure 27)** and an increase of the right ventricular ejection fraction (53 ± 3% to 60 ± 1%).

Linear regression analyses proved that correlations between an increasing RV-EDVi, RV-SVi and RV-EF with increasing lung volume during inspiration (RV-EDVi: R^2=0.992, p=0.004, RV-SVi: R^2=0.989, p=0.005, RV-EF: R^2=0.978, p=0.011) and a decreasing RV-SVi and RV-EF with decreasing lung volume during expiration (RV-SVi: R^2=0.975, p=0.013, RV-EF: R^2=0.970, p=0.015) were statistically significant.

Considering the increase in right ventricular end-diastolic volume and right ventricular stroke volume relative to an increase in lung volume by 100 ml in inspiration, there is an increase in RV-EDVi about 3.6 ml/m² i.e., about 5% and RV-SVi about 3.3 ml/m² i.e., about 8%.

3.6.2 Left ventricle

At end-diastole, visual assessment allows one to recognize that the shape of the left ventricle becomes more elliptic during inspiration, whereas at end-systole, the left ventricular shape remains unchanged and maintains its round shape during free-breathing **(Figures 25, 26)**.

The evaluation of the left ventricular volumetry showed a decrease of the left ventricular end-diastolic volume (LV-EDVi), left ventricular stroke volume (LV-SVi) and left ventricular ejection fraction (LV-EF) with increasing lung volume during inspiration for all subjects. In contrast, the left ventricular end-systolic volume (LV-ESVi) increased **(Figure 27).**

Compared to the effect of respiration on the right ventricle, the respiratory impact on the left ventricle was much less pronounced. LV-EDVi decreased by 10% during inspiration, LV-SVi decreased by 17% during inspiration, and by 6% during expiration and LV-EF decreased by 8% during inspiration.

Linear regression analysis revealed a decreasing LV-EDVi, LV-SVi, LV-EF with increasing spirometry volume during inspiration as statistically significant (LV-EDVi: R^2=0.978, p=0.011; LV-SVi: R^2=0.998, p=0.001; LV-EF: R^2=0.987, p=0.007).

During expiration, a statistically significant linear correlation was detected only for an increasing LV-ESVi (R^2=0.915, p=0.043) with increasing lung volume.

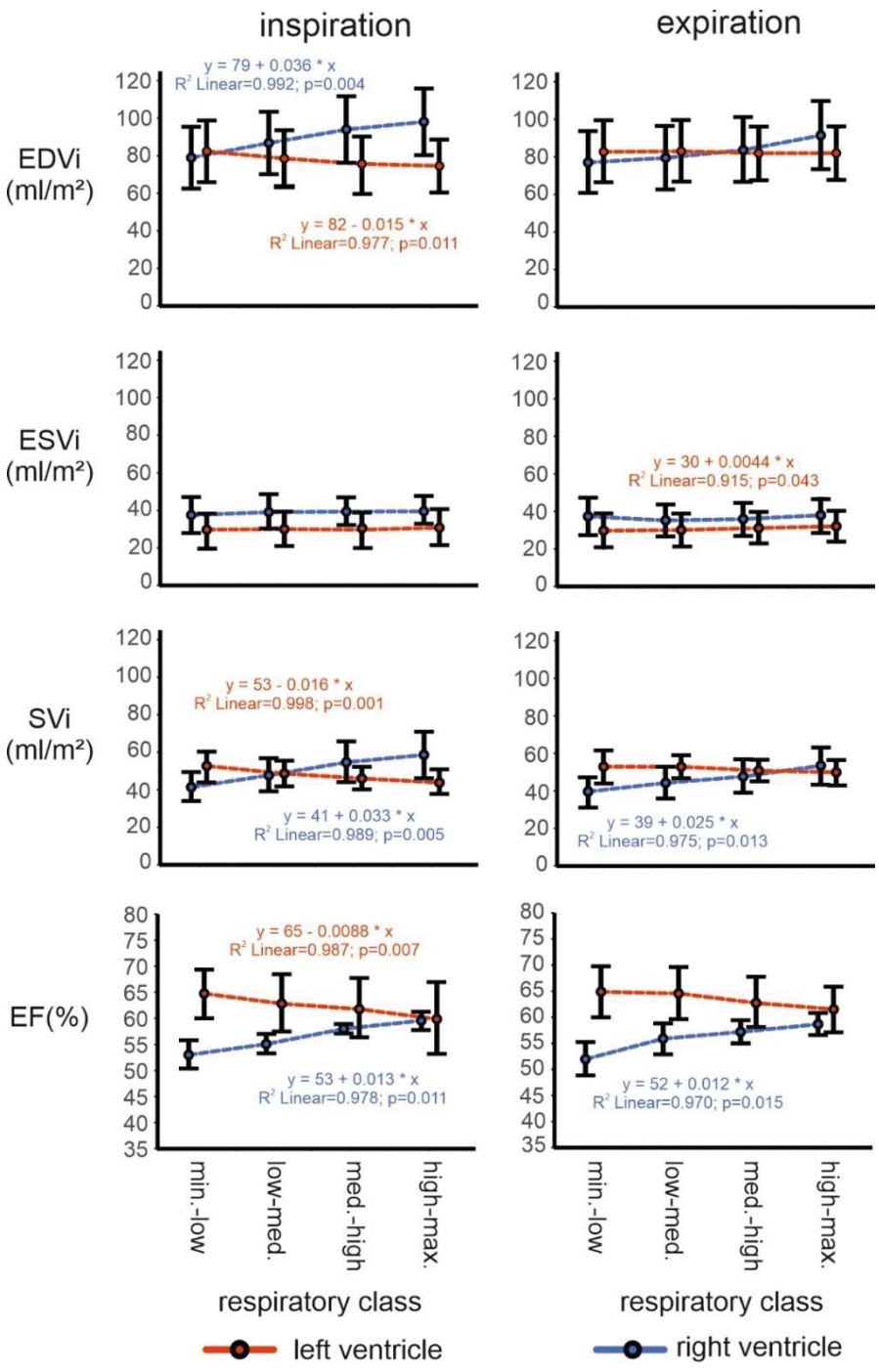

Figure 27. Ventricular volumetry.

The volume graphs demonstrate the mean results ± standard deviation of end-diastolic volume, end-systolic volume, stroke volume and ejection fraction for the left and right ventricle indexed to the body surface for all spirometry volume classes during inspiration and expiration. In the case of statistical significance for the corresponding results from linear regression analyses, formulas of the regression lines were displayed in the volume graphs. Linear regression analysis was calculated with the measured spirometry volume in ml as numerical variable instead of respiratory volume classes (modified from Röwer LM et al. (38)).

3.7 Frank-Starling mechanism

Ventricular volumetry analysis showed a linear increase in stroke volume with an increase in end-diastolic volume. This observation required an increase of >5ml/m² to become significant **(Figure 28)**.

This relationship between end-diastolic volume and stroke volume (SVi/EDVi) is known as the Frank-Starling mechanism. The results obtained showed the slope of the Frank-Starling relationship to be ~0.9 for the right ventricle in inspiration as well as expiration and ~1.1 for the left ventricle with increasing lung volume during inspiration **(Figure 28)**.

Linear regression analysis achieved highly significant results for the left ventricle with R^2=0.988 and p=0.006 during inspiration and for the right ventricle with R^2=0.998 and p=0.001 in inspiration and R^2=0.963 and p=0.019 in expiration **(Figure 28)**.

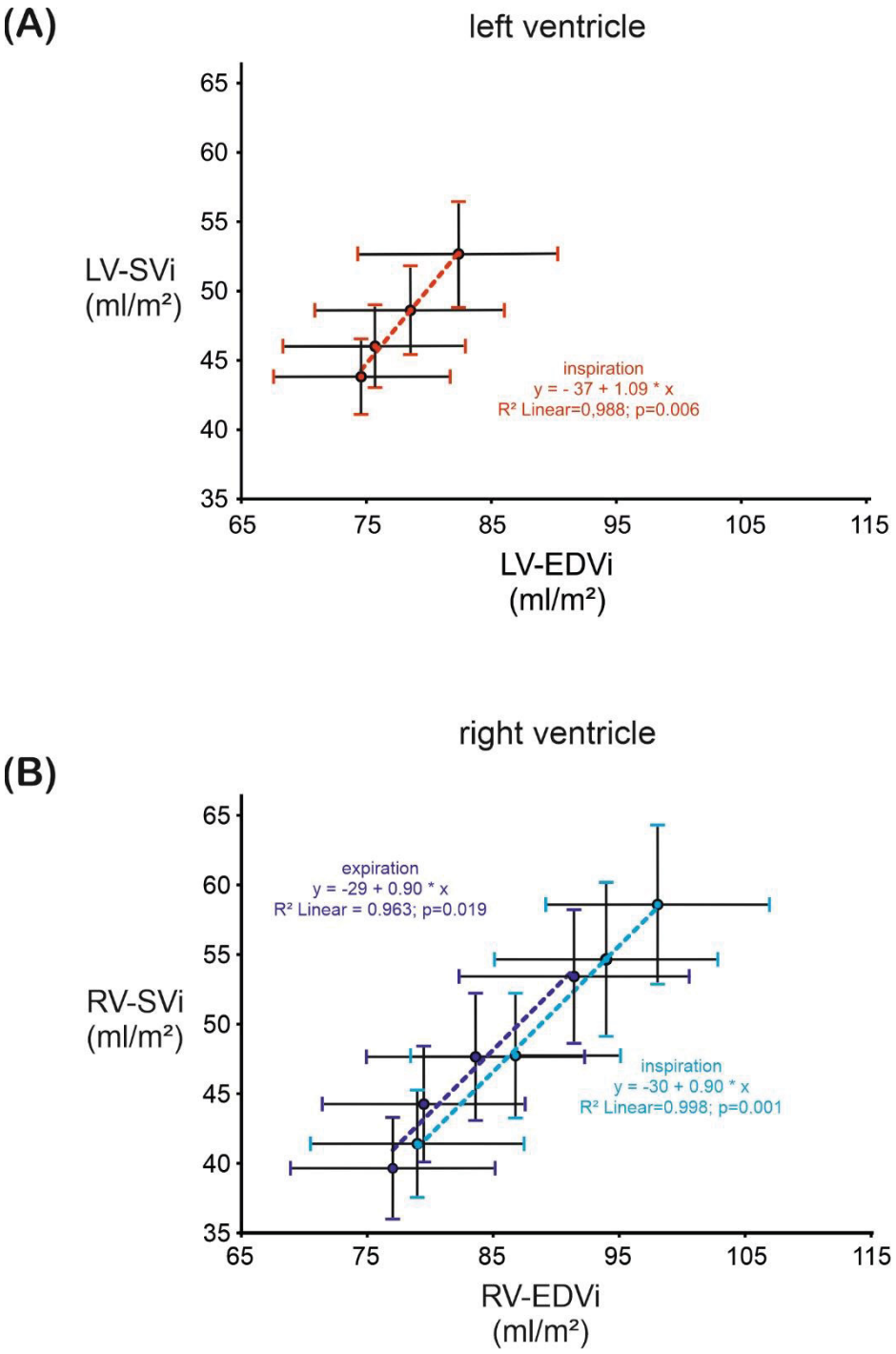

Figure 28. Frank-Starling mechanism.

The graphs demonstrate the relationship between end-diastolic volume and stroke volume for the left (A) and right (B) ventricle. Linear regression analysis results are shown in the graphs. The mean value is demonstrated as circle, the whiskers represent the standard error of the mean (modified from Röwer LM et al. (38)).

4 Discussion

Parts of the Discussion section are published in: Röwer LM, Uelwer T, Hußmann J, et al. Spirometry-based reconstruction of real-time cardiac MRI: Motion control and quantification of heart-lung interactions. Magn Reson Med. 2021;86:2692-2702. https://doi.org/10.1002/mrm.28892

The combination of real-time MRI with MR-compatible spirometry and respiratory-dependent binning to generate separate cardiac cycles for each respiratory phase resulted in a good motion control. Furthermore, the developed method provided a unique non-invasive opportunity to study physiological heart-lung interactions.

Spirometry is the gold standard for assessing pulmonary function quantitatively. MR-compatible spirometry has already been used to assess respiration in previous MR studies (35). Compared to these studies, the comfort during data acquisition with MR-compatible spirometry could be improved by implementing a well-sealed mask instead of a mouthpiece along with an adequate support by designing a customized stabilization tool to prevent the weight of the tubing and the handpiece from interfering. A questionnaire showed that this improved spirometry set-up was well tolerated and reduced comfort far less than other MR-related factors (e.g., “not being allowed to move”, “duration of the scan”, “neck and/or back pain”). Thus, in contrast to other techniques to perform respiratory binning (e.g., navigator echoes or respiratory bellows), a quantitative measurement of the lung volume while maintaining physiological conditions is feasible.

To achieve sufficient stabilization of the respiratory-induced movement, four spirometry volume classes were defined individually for each subject dependent on the lung volume range. In addition, a differentiation was made between inspiration and expiration, since both our results and previous studies showed that there are physiologically relevant differences between inspiration and expiration. During expiration, cardiac function is less influenced than during inspiration as expiration is passive and has less influence on preload as compared to the active process of inspiration (14). An even higher number of respiratory classes would have resulted in an improved image stabilization, but the data acquisition time would have increased significantly.

Due to the uneven distribution of images between different respiratory classes, the number of images needed to fill all respiratory classes exceeded the number of bins. For an average heart size, 20 slices with 900 images corresponding to an acquisition time of 10 min with a total number of 18000 images were necessary to guarantee a sufficient filling of all 4000 bins (20 slices x 25 ECG classes x four respiratory volume classes each

in inspiration and expiration). The number of images needed was approximately 4-5 times the number of bins.

Respiratory motion is a problem especially for cardiac MRI with conventional imaging techniques and long acquisition times per image. Resulting blurry and displaced images largely disturb automatic image analysis tools. The current strategy to address this issue is breath-holding. Thus, high-quality cardiac MRI in young pediatric patients as well as patients suffering from cardiac, or lung disease remains problematic (10, 11). In addition, breath-holding is unphysiological and precludes the analysis of cardiac function and the study of the left and right ventricular dimensions under physiological conditions. (13, 14, 46).

In contrast, in fast imaging techniques like real-time MRI, respiratory movement can be visualized nicely. However, the subsequent quantitative evaluation of the moving heart remains an issue. Especially the contouring of the left and right ventricle as basis for the quantification of cardiac function from real-time MRI with free-breathing is time-consuming and the semi-automatic analysis tools achieve unsatisfying results that almost preclude its actual use in clinical applications. Even if in the future, sufficient image stabilization will be provided by the evaluation software, respiratory induced through-plane motion of the heart cannot be accounted for by the image stabilization software without information on the respiratory phase. Our results from the motion control analysis revealed that spirometry-based binning is a useful tool for a reduction of respiratory motion. However, we could not demonstrate that it provides significantly better results as compared to a conventional method for respiratory motion registration (i.e., respiratory bellows).

To test the hypothesis, that MR-compatible spirometry during real-time MRI data acquisition in combination with retrospective binning is suitable for the quantification of heart lung interactions, the heart cycles from different respiratory classes were analyzed regarding the effect of respiration on the left ventricular eccentricity index as well as the respiratory impact on ventricular volumetry and dimensions. The results were then compared to the effect of respiration on cardiac function and ventricular shape already demonstrated with other, primarily invasive techniques from existing studies.

The effects of respiration on cardiac function can be assessed quickly by inspection of a midventricular slice. In this plane, the position of the ventricular septum is influenced especially by right ventricular pressure and volume load. The left ventricular eccentricity index, measuring primarily septal flattening, can be used for quantification and is an established parameter in echocardiography (47).

A significant increase in the left ventricular end-diastolic eccentricity index with increasing spirometry volume was observed in our healthy subjects. This is physiological and can be explained by a volume loading of the right ventricle with increasing preload during inspiration. In contrast, an increase in the left ventricular end-systolic eccentricity index is caused by a change of the right ventricular pressure (47). Under physiological conditions, this is not affected significantly by respiration. Therefore, as expected, our healthy subjects did not show any change of the left ventricular end-systolic eccentricity index.

Although the eccentricity index of a midventricular slice can be determined easily and quickly, it cannot replace the volumetry analysis of the heart sufficiently, especially given the respiratory-dependent through-plane motion of the heart. A true volumetry analysis was made possible by binning the real-time MR images of every slice in different respiratory dependent heart-cycles. This resulted in eight stacks of images that could be evaluated separately, similarly to images obtained during breath-holding at different time points during the breathing cycle.

Evaluation of ventricular volumetry showed that even quiet, free-breathing results in significant changes in right and left ventricular volumes in healthy subjects. This observation underlines that mixing images from different respiratory phases is inadequate for the analysis of cardiac function, as already shown in previous studies (14).

An increasing right ventricular end-diastolic volume and stroke volume with increasing lung volume during inspiration has already been demonstrated in previous invasive physiological studies (48, 49, 50). This is caused by a change of ventricular preload (14) and paralleled by an increase in stroke volume explained by the Frank-Starling law (51).

The increase in the end-diastolic volume of the right ventricle is accompanied by a less pronounced decrease in the left ventricular end-diastolic volume. This respiratory effect on the left ventricle has also been described before by different methods (14, 50). However, the underlying mechanism of this decrease is still a matter of debate (14, 52, 53). Common explanations suggest that the decrease in end-diastolic volume results from a decrease in left ventricular compliance as well as an increase in left ventricular afterload (14, 27, 53).

The Frank-Starling mechanism is one of the most fundamental concepts of cardiopulmonary physiology and describes an increase of stroke volume with increasing end-diastolic volume (51). We could confirm that even normal breathing results in an increase of the right ventricular end-diastolic volume during inspiration and a decrease

during expiration. The left ventricular end-diastolic volume decreases during inspiration. These physiological modifications of the end-diastolic volume enabled us to quantify the relationship between end-diastolic volume and stroke volume non-invasively. Such an investigation of the Frank Starling law (54, 55) was mostly done with invasive methods or cardiac models in previous studies (56, 57). It should be helpful for understanding and analyzing heart-lung interactions in healthy subjects and in patients with congenital or acquired heart disease to study this non-invasively.

4.1 Conclusions

Real-time MRI during free-breathing in combination with MR-compatible spirometry and retrospective ECG- and respiratory-based binning is feasible and improves the evaluation of cardiac real-time volumetry. In addition, it offers the unique opportunity to study heart-lung interactions and to investigate the Frank-Starling law non-invasively.

Spirometry is the gold standard for measuring quantitative respiratory data. MR-compatible spirometry was well tolerated in healthy full-aged subjects, its use in adolescents and adult patients with congenital or acquired heart disease could be conceivable. Nevertheless, the use of spirometry in small children remains difficult. Therefore, an alternative non-invasive method for providing quantitative respiratory flow and lung volume during real-time MRI would be desirable.

Future studies could investigate heart-lung interactions in healthy subjects under different conditions e.g., deep breathing and designated breathing maneuvers but also to analyze heart-lung interactions in patients with pathophysiologic circulation situations e.g., patients with congenital or acquired heart disease.

The investigation of the Frank-Starling curve in healthy subjects resulted in physiological values. Especially in patients with heart failure, the non-invasive investigation of the Frank-Starling relationship could potentially improve the diagnosis and help to monitor the therapy of this highly relevant disease.

References

1. Mannaerts HF, Van Der Heide JA, Kamp O, et al. Quantification of left ventricular volumes and ejection fraction using freehand transthoracic three-dimensional echocardiography: comparison with magnetic resonance imaging. J Am Soc Echocardiogr. 2003;16(2):101-9.
2. Constatine G, Shan K, Flamm SD, et al. Role of MRI in clinical cardiology. The Lancet. 2004;363:2162:2171.
3. Deutsch HJ, Smolorz J, Sechtem U, et al. Cardiac function by magnetic resonance imaging. Int J Card Imaging. 1988;3:3-11.
4. Matsumura K, Nakase E, Haiyama T, et al. Determination of Cardiac Ejection Fraction and Left Ventricular Volume: Contrast-Enhanced Ultrafast Cine MR Imaging vs IV Digital Subtraction Ventriculography. Am J Roentgenol. 1993;160:979-985.
5. Markiewicz W, Sechtem U, Higgings CB. Evaluation of the right ventricle by MRI. Am Heart J. 1987;113:8.
6. Mostbeck GH, Caputo GR, Higgings CB. MR Measurement of Blood Flow in the Cardiovascular System. Am J Roentgenol. 1992;159:453-461.
7. Higgings CB, Byrd BF, Farmer DW, et al. Magnetic resonance imaging in patients with congenital heart disease. Circulation. 1984;70:851-860.
8. Didier D, Higgings CB, Fisher M et al. Congenital heart disease: gated MR imaging in 72 patients. Radiology. 1986;158:227-235.
9. Brown DW, Gauvreau K, Powell AJ, et al. Cardiac Magnetic Resonance Versus Routine Cardiac Catheterization Before Bidirectional Glenn Anastomosis in Infants With Functional Single Ventricle A Prospective Randomized Trial. Circulation. 2007;116:2718:2725.
10. Gay SB, Sistrom CL, Holder CL, et al. Breath-holding capability of adults. Implications for spiral computed tomography, fast-acquisition magnetic resonance imaging, and angiography. Invest Radiol. 1994;9:848-851.
11. Funk E, Thunberg P, Anderzen-Carlsson A. Patients' experiences in magnetic resonance imaging (MRI) and their experiences of breath holding techniques. J Adv Nurs. 2014;70:1880-1890.
12. Hong SK, Lin YC, Lally DA, et al. Alveolar gas exchanges and cardiovascular functions during breath holding with air. J Appl Physiol. 1971; 4:540-547.
13. Ferrigno M, Hickey DD, Linér MH, et al. Cardiac performance in humans during breath holding. J Appl Physiol. (1985). 1986; 60(6):1871-7.
14. Magder S. Heart-Lung interaction in spontaneous breathing subjects: the basics. Ann Transl Med. 2018; 18: 348.
15. Mahmood SS, Pinsky MR. Heart-lung interactions during mechanical ventilation: the basics. Ann Transl Med.2018;6:349.
16. Ridgway JP. Cardiovascular magnetic resonance physics for clinicans: part I. J. Cardiovasc. Magn. Reson. 2010;12:71.
17. Bluemke DA, Boxerman JL, Atalar E, et al. Segmented K-space cine breath-hold cardiovascular MR imaging: Part 1. Principles and technique. Am J Roentgenol. 1997;169:395-400.

18. Kramer CM, Barkhausen J, Flamm SD, et al. Standardized cardiovascular magnetic resonance (CMR) protocols 2013 update. J. Cardiovasc. Magn. Reson. 2013;15:91.
19. Fratz S, Chung T, Greil GF, Samyn MM et al. Guidelines and protocols for cardiovascular magnetic resonance in children and adults with congenital heart disease: SCMR expert consensus group on congenital heart disease. J. Cardiovasc. Magn. Reson. 2013;15:51.
20. Uecker M, Zhang S, Frahm J. Nonlinear inverse reconstruction for real-time MRI of the human heart using undersampled radial FLASH. Magn Reson Med. 2010;63:1456–62.
21. Haase A, Frahm J, Matthaei D, et al. FLASH Imaging. Rapid NMR Imaging using low flip-angle pulses. J. Magn. Reson. Imaging. 1986;67:258-266.
22. Frahm J, Voit D, Uecker M. Real-Time Magnetic Resonance Imaging Radial Gradient-Echo Sequences With Nonlinear Inverse Reconstruction. Invest Radiol. 2019;54:757–766.
23. Voit D, Zhang S, Unterberg-Buchwald C, et al. Real-time cardiovascular magnetic resonance at 1.5 T using balanced SSFP and 40 ms resolution. J. Cardiovasc. Magn. Reson. 2013;15:79.
24. Thiele H, Paetsch I, Schnackenburg B, et al. Improved Accuracy of Quantitative Assessment of Left Ventricular Volume and Ejection Fraction by Geometric Models with Steady-State Free Precession. J. Cardiovasc. Magn. Reson. 2002;327-339.
25. Voerhoff K, Mitchell JR. Cardiopulmonary physiology: why the heart and lungs are inextricably linked, Adv Physiol. Educ. 2017;41:348-353.
26. Kobirumaki-Shimozawa F, Inoue T, Shintani SA, et al. Cardiac thin filament regulation and the Frank-Starling mechanism. J Physiol Sci. 2014;64(4):221-232.
27. Wise RA, Robotham JL, Summer WR. Effects of spontaneous ventilation on the circulation. Lung. 1981;159:175–186.
28. Summer WR, Permutt S, Sagawa K, et al. Effects of spontaneous respiration on canine left ventricular function. Circ Res. 1979;45:719-728.
29. Sequeira V, van der Velden J. Historical perspective on heart function: the Frank–Starling Law. Biophys Rev. 2015;7:421–447.
30. Kuhtz-Buschbeck JP, Lie RK, Schaefer J, et al. Reassessing Diagrams of Cardiac Mechanics: From Otto Frank and Ernest Starling to Hiroyuki Suga. Perspect Biol Med. 2016;59(4):471-490.
31. Scott AD, Keegan J, Firmin DN. Motion in cardiovascular MR imaging. Radiology. 2009;250:331-351.
32. Runge VM, Richter JK, Heverhagen JT. Motion in Magnetic Resonance: New Paradigms for Improved Clinical Diagnosis. Invest Radiol. 2019;54:383-395.
33. Santelli C, Nezafat R, Goddu B, et al. Respiratory bellows revisited for motion compensation: preliminary experience for cardiovascular MR. Magn Reson Med. 2011;65:1097–1102.
34. Nehrke K, Manke D. Advanced Navigator Techniques. Int. j. bioelectromagn. 2000;2:248-254.
35. Eichinger M, Puderbach M, Smith HJ, et al. Magnetic-resonance-compatible-spirometry: principle, technical evaluation and application. Eur Respir J. 2007;30:972-979.

36. Gelfand R, Lambertsen CJ, Peterson RE, et al. Pneumotachograph for flow and volume measurement in normal and dense atmospheres. J. Appl. Physiol. 1976;41:120-124.
37. Kokki T, Klén R, Noponen T, et al. Linear relation between spirometric volume and the motion of cardiac structures: MRI and clinical PET study. J. Nucl. Cardiol. Volume. 2016;23:475-485.
38. Röwer LM, Uelwer T, Hußmann J, et al. Spirometry-based reconstruction of real-time cardiac MRI: Motion control and quantification of heart-lung interactions. Magn Reson Med. 2021;86:2692-2702.
39. Chen S, Hu P, Gu Y, et al. Impact of patient comfort on diagnostic image quality during PET/MR exam: A quantitative survey study for clinical workflow management. J Appl Clin Med Phys. 2019;20:184-192.
40. Harris CR, Millman KJ, van der Walt SJ, et al. Array programming with NumPy. Nature. 2020;585:357-362.
41. Mason D, scaramallion, rhaxton, et al. Pydicom/pydicom: V1. 4. 0. January 20, 2020. Available at: https://doi.org/10.5281/zenodo.3614042.
42. Schulz-Menger J, Bluemke DA, Bremerich J, et al. Standardized image interpretation and post processing in cardiovascular magnetic resonance: Society for Cardiovascular Magnetic Resonance (SCMR) Board of Trustees Task Force on Standardized Post Processing. J Cardiovasc Magn Reson. 2013;15:35.
43. Paknezhad M, Marchesseau S, Brown MS. Automatic basal slice detection for cardiac analysis. J Med Imaging (Bellingham). 2016;3:034004.
44. Marchesseau S, Ho JXM, Totman JJ. Influence of the short-axis cine acquisition protocol on the cardiac function evaluation: A reproducibility study. Eur J Radiol Open. 2016;3:60-66.
45. van der Ven JPG, Sadighy Z, Valsangiacomo Buechel ER, et al. Multicentre reference values for cardiac magnetic resonance imaging derived ventricular size and function for children aged 0-18 years. Eur Heart J Cardiovasc Imaging. 2020;21:102-113.
46. Paulev P, Wetterqvist H. Cardiac output during breath-holding in man. Scand J Clin Lab Invest. 1968;22:115-123.
47. Ryan T, Petrovic O, Dillon J, Feigenbaum H, Conley MJ, Armstrong WF. An echocardiographic index for separation of right ventricular volume and pressure overload. J Am Coll Cardiol. 1985;5:918-927.
48. Guyton AC, Lindsey AW, Abernathy B, Richardson T. Venous return at various right atrial pressures and the normal venous return curve. Am J Physiol. 1957;189:609-615.
49. Shuler RH, Ensor C, Ginning RE, Moss WG,Johnson V. The differential effects of respiration on the left and right ventricles. Am J Physiol. 1942;137:620-627.
50. Claessen G, Claus P, Delcroix M, et al. Interaction between respiration and right versus left ventricular volumes at rest and during exercise: a real-time cardiac magnetic resonance study. Am J Physiol Heart Circ Physiol. 2014;306:H816-H824.
51. Delicce AV, Makaryus AN. Physiology, Frank Starling Law. In: StatPearls. Treasure Island (FL): StatPearls Publishing;2020.
52. Korperich H, Barth P, Gieseke J, et al. Impact of respiration on stroke volumes in paediatric controls and in patients after fontan procedure assessed by MR real-time phase-velocity mapping. Eur Heart J Cardiovasc Imaging. 2015;16:198-209.

53. Ruskin J, Bache RJ, Rembert JC, Greenfield Jr JC. Pressure-flow studies in man: effect of respiration on left ventricular stroke volume. Circulation. 1973;48:79-85.
54. Frank O. Zur Dynamik des Herzmuskels. Ztschr Biol. 1895;32:370.
55. Starling EH. The linacre lecture on the law of the heart given at Cambridge, 1915. Nature 1918;101.
56. Schneider NS, Shimayoshi T, Amano A, et al. Mechanism of the Frank-Starling law--a simulation study with a novel cardiac muscle contraction model that includes titin and troponin I. J Mol Cell Cardiol. 2006;41:522-536.
57. Feneley MP, Skelton TN, Kisslo KB, et al. Comparison of preload recruitable stroke work, end-systolic pressure-volume and dP/dtmax-end-diastolic volume relations as indexes of left ventricular contractile performance in patients undergoing routine cardiac catheterization. J Am Coll Cardiol. 1992;19:1522-1530.

Supplements

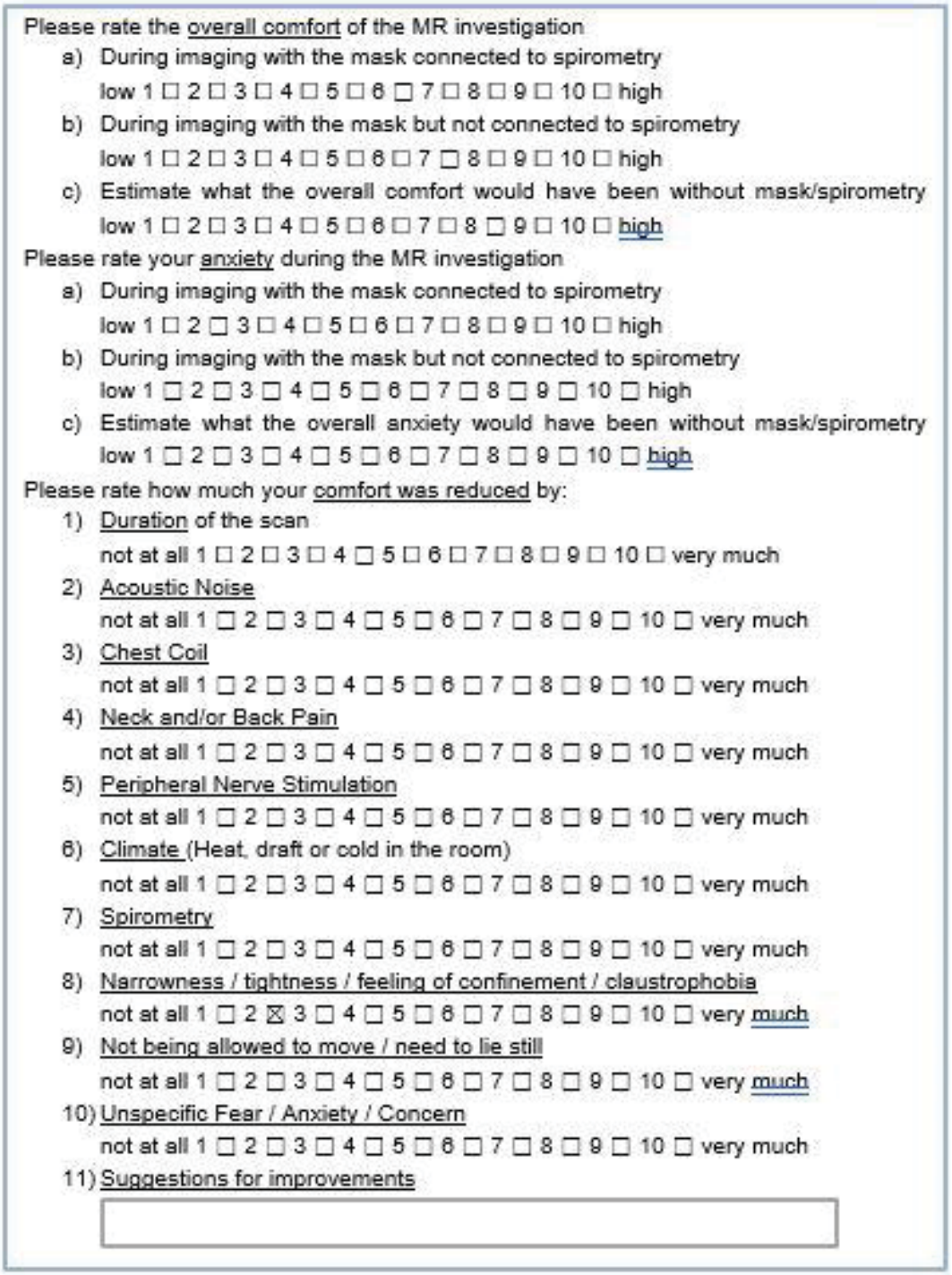

Please rate the overall comfort of the MR investigation

a) During imaging with the mask connected to spirometry
low 1 ☐ 2 ☐ 3 ☐ 4 ☐ 5 ☐ 6 ☐ 7 ☐ 8 ☐ 9 ☐ 10 ☐ high

b) During imaging with the mask but not connected to spirometry
low 1 ☐ 2 ☐ 3 ☐ 4 ☐ 5 ☐ 6 ☐ 7 ☐ 8 ☐ 9 ☐ 10 ☐ high

c) Estimate what the overall comfort would have been without mask/spirometry
low 1 ☐ 2 ☐ 3 ☐ 4 ☐ 5 ☐ 6 ☐ 7 ☐ 8 ☐ 9 ☐ 10 ☐ high

Please rate your anxiety during the MR investigation

a) During imaging with the mask connected to spirometry
low 1 ☐ 2 ☐ 3 ☐ 4 ☐ 5 ☐ 6 ☐ 7 ☐ 8 ☐ 9 ☐ 10 ☐ high

b) During imaging with the mask but not connected to spirometry
low 1 ☐ 2 ☐ 3 ☐ 4 ☐ 5 ☐ 6 ☐ 7 ☐ 8 ☐ 9 ☐ 10 ☐ high

c) Estimate what the overall anxiety would have been without mask/spirometry
low 1 ☐ 2 ☐ 3 ☐ 4 ☐ 5 ☐ 6 ☐ 7 ☐ 8 ☐ 9 ☐ 10 ☐ high

Please rate how much your comfort was reduced by:

1) Duration of the scan
not at all 1 ☐ 2 ☐ 3 ☐ 4 ☐ 5 ☐ 6 ☐ 7 ☐ 8 ☐ 9 ☐ 10 ☐ very much

2) Acoustic Noise
not at all 1 ☐ 2 ☐ 3 ☐ 4 ☐ 5 ☐ 6 ☐ 7 ☐ 8 ☐ 9 ☐ 10 ☐ very much

3) Chest Coil
not at all 1 ☐ 2 ☐ 3 ☐ 4 ☐ 5 ☐ 6 ☐ 7 ☐ 8 ☐ 9 ☐ 10 ☐ very much

4) Neck and/or Back Pain
not at all 1 ☐ 2 ☐ 3 ☐ 4 ☐ 5 ☐ 6 ☐ 7 ☐ 8 ☐ 9 ☐ 10 ☐ very much

5) Peripheral Nerve Stimulation
not at all 1 ☐ 2 ☐ 3 ☐ 4 ☐ 5 ☐ 6 ☐ 7 ☐ 8 ☐ 9 ☐ 10 ☐ very much

6) Climate (Heat, draft or cold in the room)
not at all 1 ☐ 2 ☐ 3 ☐ 4 ☐ 5 ☐ 6 ☐ 7 ☐ 8 ☐ 9 ☐ 10 ☐ very much

7) Spirometry
not at all 1 ☐ 2 ☐ 3 ☐ 4 ☐ 5 ☐ 6 ☐ 7 ☐ 8 ☐ 9 ☐ 10 ☐ very much

8) Narrowness / tightness / feeling of confinement / claustrophobia
not at all 1 ☐ 2 ☒ 3 ☐ 4 ☐ 5 ☐ 6 ☐ 7 ☐ 8 ☐ 9 ☐ 10 ☐ very much

9) Not being allowed to move / need to lie still
not at all 1 ☐ 2 ☐ 3 ☐ 4 ☐ 5 ☐ 6 ☐ 7 ☐ 8 ☐ 9 ☐ 10 ☐ very much

10) Unspecific Fear / Anxiety / Concern
not at all 1 ☐ 2 ☐ 3 ☐ 4 ☐ 5 ☐ 6 ☐ 7 ☐ 8 ☐ 9 ☐ 10 ☐ very much

11) Suggestions for improvements

Supplement 1. Comfort survey.

A standardized questionnaire was used to evaluate the degree of anxiety and comfort during the real-time MRI data acquisition (modified from Chen, S. et al. (39)).

Danksagung

Besonders bedanken möchte ich mich bei meinem Doktorvater Prof. Frank Pillekamp für die herausragende Betreuung, großartige Zusammenarbeit, Hilfestellung und Unterstützung bei allen Fragen. Ohne Ihre Betreuung wäre diese Arbeit nicht möglich gewesen. Ich habe mich sehr gefreut von Ihnen lernen zu dürfen.

Ebenfalls bedanken möchte ich mich bei Dr. Dirk Klee für die großartige Zusammenarbeit, Betreuung und Hilfe und für die Unterstützung bei allen Fragen und organisatorischen Angelegenheiten von Seiten der Kinderradiologie.

Ich danke Evelyn Radomsky für das geduldige Beibringen und die Unterstützung bei der Herz-MRT Messung und die schöne Zeit, die wir zusammen im MRT 3 verbracht haben.

Danke an Janina Hußmann und Halima Malik für die Hilfe, gegenseitige Unterstützung, tolle Zusammenarbeit und vor allem für die vielen lustigen Momente die wir als Doktorandinnen zusammen erlebt haben.

Ebenfalls bedanken möchte ich mich bei Tobias Uelwer und Prof. Stefan Harmeling für die großartige Zusammenarbeit und besonders für die Umsetzung und Programmierung des Informatikanteils und die Hilfe und Unterstützung bei allen Problemen von Seiten der Informatik.

Danke an Priv. Dozentin Dr. Monika Eichinger und Prof. Mark Wielpütz und Frau Ginschel für den schönen Tag in Heidelberg, die tolle Zusammenarbeit und die Ausleihe sowie Erklärung der MRT-kompatiblen Spirometrie sowie die Unterstützung bei der Organisation des Leihvertrags.

Vielen Dank an Prof. Jens Frahm und Dr. Dirk Voit für die Unterstützung und Hilfe bei allen Fragen zur Echtzeit-MRT.

Ich danke dem Pflegeteam der KA03 im Zentrum für Kinder und Jugendmedizin des Universitätsklinikum Düsseldorf, besonders Ulla Pfeiffer und Silvia Höltermann für die Hilfe beim pflegerischen Umgang mit dem Spirometer und dafür, dass ich bei Fragen immer zu euch kommen konnte.

Vielen Dank Herrn Kieslich für die Unterstützung und das offene Ohr bei vielen organisatorischen und technischen Fragen und Problemen.

Ebenfalls bedanken möchte ich mich bei Prof. Wittsack für die Unterstützung und Hilfe bei technischen Fragen und besonders für die Hilfestellung beim MRT Signal Logging.

Viele Dank an Marcus Welsh für die sprachlichen Korrekturen sowohl bei der Publikation als auch bei der Dissertation.

Vielen Dank an alle freiwilligen Probanden, die sich für die Herz-MRT Messung bereiterklärt haben.

Danke dem gesamten Team des MRT 3 und der Kinderradiologie dafür, dass ich selbstständig das MRT nutzen durfte.

Besonders bedanken möchte ich mich bei der Elterninitiative Kinderkrebsklinik für das Funding.

Vielen Dank an Prof. Mayatepek und Frau Dietzen für die Hilfe bei der Organisation und Finanzierung des Spirometrie Zubehörs.

Ich danke Prof. Antoch für das Gutachten und die Unterstützung von Seiten der Radiologie.

Vielen Dank an meine Freunde und vor allem an meine Familie für die Unterstützung während der gesamten Zeit der Doktorarbeit und der Unterstützung während des Medizinstudiums.